Theory of Auger Neutralization of Ions at the Surface of a Diamond-Type Semiconductor

HOMER D. HAGSTRUM
Bell Telephone Laboratories, Murray Hill, New Jersey
(Received November 21, 1960)

The two-electron, Auger-type transitions which occur when an ion of sufficiently large ionization energy is neutralized at the atomically clean surface of a diamond-type semiconductor are discussed. Consideration of the basic elements of the problem leads to a computing program which enables one to calculate the total electron yield and kinetic energy distribution of ejected electrons in terms of a number of parameters. It is possible to account for the experimental results for singly-charged noble gas ions incident on the (111) faces of Si and Ge and the (100) face of Si. The fit of theory to experiment is unique in its principal features yielding numerical results concerning: (1) the state density function for the valence bands of Si and Ge, (2) the energy dependence of the matrix element as it is determined by symmetry of the valence band wave functions, (3) the effective ionization energy near the solid surface, (4) energy broadening, and (5) electron escape over the surface barrier. Over-all width of the valence band is found to be 14–16 ev for both Si and Ge. Width of the degenerate p bands is 5.1 ev in Si, 4.3 ev in Ge. The matrix element for p-type valence electrons is 0.3 times that for s-type valence electrons. Effective ionization energy is 2.2 ev less than the free-space value for 10-ev He^+ ions and decreases linearly with ion velocity. Energy broadening is small for 10-ev ions and increases approximately linearly with ion velocity. Probability of electron escape is several times that predicted for an isotropic distribution of excited electrons incident on a plane surface barrier. A general theory of Auger neutralization is given in which the conclusions of the fit to experiment are interpreted. Investigation of the matrix element as a Coulomb interaction integral involving wave functions whose general characteristics are known but which are not explicitly evaluated leads to an understanding of its principal dependences on energy and angle.

I. INTRODUCTION

A THEORY of the Auger-type electronic transitions, which occur when an ion is neutralized at a solid surface, is presented in this paper for the case of the diamond-type semiconductor. It has been developed in an attempt to understand the experimental results for noble gas ions incident on atomically clean surfaces of germanium and silicon.[1]

Massey,[2] Shekhter,[3] and Cobas and Lamb[4] have treated the two-stage process consisting of neutralization of the ion to an excited state by resonance tunneling at a metal surface followed by de-excitation of the excited atom in a two-electron, Auger-type transition. Shekhter[3] has also discussed the direct neutralization to the ground state in the two-electron, Auger-type transition with which the present paper is concerned. In each of these theories the attempt was made to calculate matrix elements from assumed wave functions. The results are of limited value because the wave functions were not accurate and because a number of very important elements of the problem were ignored.

In the author's previously published theory of Auger ejection of electrons from metals[5] a computer calculation was made of the kinetic energy distribution and total yield of ejected electrons. In this work a number of the elements previously ignored were incorporated in the theory. These are: (1) energy distribution of initial electronic states in the solid, (2) dependence of the matrix element on the angle which the excited electron's velocity makes with the surface normal and the effect of this on the probability of escape from the solid, (3) variation of energy levels in the ion as it approaches the solid surface, (4) the fact that ion neutralization occurs over a range of distances from the surface, (5) finite lifetime of the initial state, and (6) the role of resonance tunneling to an excited state in determining the partition between Auger neutralization and Auger de-excitation processes.

In the theory for metals the following basic facts concerning the Auger neutralization process were established.

(1) The magnitude of electron yield is determined by the ionization energy, the initial state density distribution, and the probability of electron escape. It is not determined, as Shekhter assumed,[3] by the integrated transition probability over all distances from the surface, which is unity.

(2) The form of the kinetic energy distribution is determined by an integral transform of the energy level distribution in the filled band of the solid in which the electrons initially reside as was discussed for another Auger process by Lander.[6]

(3) The role of the ion's incident kinetic energy is to determine energy level shift in the atom and energy broadening by determining the average distance from the surface at which the process occurs.

More recently, Sternberg[7] has again attempted to calculate matrix elements from assumed wave functions for the resonance tunneling and Auger processes. Considerable improvement over the earlier calculations of a

[1] H. D. Hagstrum, Phys. Rev. **119**, 940 (1960).
[2] H. S. W. Massey, Proc. Cambridge Phil. Soc. **26**, 386 (1930); **27**, 469 (1931).
[3] S. S. Shekhter, J. Exptl. Theoret. Phys. (U.S.S.R) **7**, 750 (1937).
[4] A. Cobas and W. E. Lamb, Jr., Phys. Rev. **65**, 327 (1944).
[5] H. D. Hagstrum, Phys. Rev. **96**, 336 (1954).
[6] J. J. Lander, Phys. Rev. **91**, 1382 (1953).
[7] D. Sternberg, Ph.D. dissertation, Columbia University, 1957 (unpublished); available from University Microfilms, Ann Arbor, Michigan.

TABLE I. Definitions of notation.[a]

e^-	free electron.	$u_g(1)$	wave function of electron 1 in atomic ground state.
e_S^-	electron inside semiconductor.	$u_e(2)$	wave function of electron 2 when excited to energy ϵ_k if it is transmitted across surface barrier.
n	number of electrons in the valence band used in Eq. (89).	$u_e'(2)$	wave function of electron 2 excited to energy ϵ_k if it is reflected at surface barrier.
ϵ, ϵ', ϵ''	energy of valence electron measured from bottom of valence band.	$r_t(\epsilon',\epsilon'',\theta,\varphi,s)$	transition rate for elemental Auger process.
Δ	$(\epsilon'+\epsilon'')/2$.	$R_t(s)$	total transition rate.
ϵ_k	energy above bottom of valence band of excited electron inside solid.	$P_0(s,v_0)$	probability that ion of velocity v_0 will reach s without undergoing Auger neutralization.
$\delta\epsilon_k$	uncertainty in ϵ_k introduced by the Heisenberg uncertainty principle.	$P_t(s,v_0)ds$	probability that ion approaching surface with velocity v_0 will undergo Auger neutralization in ds at s.
ϵ_0	energy of vacuum level above bottom of valence band.	$P_k(\epsilon_k,s)d\epsilon_k$	probability that a process occurring with incident ion at s will produce excited electron in $d\epsilon_k$ at ϵ_k.
ϵ_c	energy of bottom of conduction band above bottom of valence band.	$P_\Omega(\theta,\epsilon_k,s)d\Omega$	probability that excited electron of energy ϵ_k formed at s has velocity in $d\Omega=\sin\theta d\theta d\varphi$ at θ, φ.
ϵ_v	energy of top of valence band above its bottom (i.e., total width of valence band).	$I(\delta\epsilon_k,s)d(\delta\epsilon_k)$	probability that the energy of an excited electron formed by a process occurring at s will be uncertain by an amount $\delta\epsilon_k$ due to the Heisenberg uncertainty principle.
p	ϵ/ϵ_v at bottom of degenerate p band making width of degenerate p band $(1-p)\epsilon_v$.	$P_e(\epsilon_k)$, $P_e(E_k)$	probability that excited electron at $\epsilon_k=E_k+\epsilon_0$ will escape from solid.
E_k	kinetic energy of particle (atom, ion, electron) outside solid measured from zero at the vacuum level. Nature of particle may be expressed in parentheses after the symbol as in $E_k(e^-)$, $E_k(\mathrm{He}^+)$.	α, β	parameters in the P_e function.
		A, a	parameters in exponential transition rate $R_t(s)=A\exp(-as)$.
E_i	free space ionization energy.	B, b	parameters in exponential repulsive interaction term $B\exp(-bs)$ (subscript i denotes ion, n denotes normal atom).
E_i', $E_i'(s)$	effective ionization energy at a distance s from the solid surface.	$N_v(\epsilon)$	density of states in valence band.
$E(n,S)$	energy of interaction between normal atom and solid surface.	$N_v'(\epsilon)$	effective density of states in valence band which includes dependence of matrix element on energy.
$E(i,S)$	energy of interaction between ion and solid surface.	$q(\epsilon)$	$N_v'(\epsilon)/N_v(\epsilon)$ which specifies variation of matrix element with ϵ.
$\delta(\epsilon)$	Dirac δ function on energy.	r	factor by which a p electron is less effective than an s electron in the Auger neutralization process.
s	distance of particle from plane of outermost nuclei of solid.	$N_c(\epsilon)$	density of states in conduction band.
s_m	distance at which $P_t(s,v_0)$ is maximum.	$N_i(\epsilon_k)$	distribution in energy of excited electrons inside solid.
r_{12}	distance between electrons 1 and 2.	$N_0(E_k)$	distribution in energy of ejected electrons outside solid.
v_0	incident velocity of particle toward solid.	$T(\epsilon)$	Auger transform of $N_v'(\epsilon)$ [Eq. (16)].
θ	angle between surface normal and velocity of excited electron inside solid.	$T_b(\epsilon)$	broadened Auger transform [Eq. (17)].
θ_c	maximum θ for escape over surface barrier.	$\varphi_\sigma(x)$	broadening function taken to be Gaussian in this work.
φ	azimuthal angle about surface normal.	σ	parameter determining spread of Gaussian function.
H_{fi}	matrix element of Auger transitions.	σ_1	σ factor from variation of energy levels.
H', H''	"elemental" matrix elements derived from each other by electron exchange [Eqs. (49) and (50)].	σ_2	σ factor from Heisenberg principle.
m	H''/H'.	$W(F)$	width at half maximum of the function F.
H_1, H_2	average values of H' for $\theta<\theta_c$ and $\theta>\theta_c$, respectively.	γ_i	total electron yield in electrons per ion.
f	H_1/H_2.	κ	dielectric constant of the semiconductor.
α	$1-1/f^2$.		
$u_v'(1)$, $u_v''(2)$	wave functions of electrons 1 and 2 at ϵ' and ϵ'' in the valence band, respectively.		

[a] Notation introduced at only one place in the paper is not included in this table.

similar nature has been made, but it still appears to be impossible to calculate the total electron yield in this way.

The present work for the diamond-type semiconductors may be considered to be an extension of the author's previous theory for metals. A computer calculation of the total yield and kinetic energy distribution is again made in terms of the basic parameters of the problem. In order to fit the theory to the experiment in this case, however, it is necessary also to take account

of the variation of the matrix element with energy of the initial states. Furthermore, the greater width of the filled band in Ge and Si as compared to W makes it probable that resonance tunneling to the ground state can occur for the singly-charged noble gas ions of ionization energy less than that of He^+.

In the present paper the experimental facts to be explained are first presented (Sec. II) and the electronic transitions are specified (Sec. III). Consideration of the basic elements of the Auger neutralization process (Sec. IV) leads to the computer program (Sec. V) for calculating the kinetic energy distribution of ejected electrons and the total electron yield in terms of the essential parameters. Solutions based on simplifying assumptions which are progressively removed are presented in Sec. VI. Energy broadening is then included in the theory (Sec. VII) and uniqueness of the theoretical fit discussed (Sec. VIII). Solutions previously made for He^+ ions of various kinetic energies incident on the (111) face of Ge are then extended to the other singly-charged noble gas ions and to the Si(111) and Si(100) crystal faces (Sec. IX). The basic conclusions demanded by the fit of theory to experiment are summarized in Sec. X. In Secs. XI–XV a general theory of the phenomenon is presented in terms of which these conclusions are interpreted. The state density functions determined for the Si and Ge valence bands are discussed in Sec. XVI and surface effects in Sec. XVII. Notation used generally throughout the paper is defined in Table I.

II. EXPERIMENTAL FACTS TO BE EXPLAINED

The phenomenon we are attempting to understand is the release of electrons from a diamond-type semiconductor which accompanies the neutralization of an ion of sufficiently large ionization energy at the semiconductor surface.[8] The basic experimental information concerning this phenomenon comprises the kinetic energy distribution, $N_0(E_k)$, and its integral, the total yield, γ_i. These quantities are found to depend specifically upon the nature of the solid and the state of its surface as well as the nature of the ion and its incident kinetic energy.

In this paper we shall concern ourselves with atomically clean and atomically smooth surfaces of the elemental semiconductors silicon and germanium. Thus we shall not attempt to include in the theory the effects of surface steps, surface terminations of dislocations, foreign atoms adsorbed on the surface, or any other surface "defect". In the experiments atomic cleanliness has been demonstrated but the surfaces used certainly had steps and dislocations on them. For the (111) faces there is evidence that reasonably large areas of the surface are most likely atomically plane. Thus on most encounters the surface should appear to be atomically smooth to the ion which senses only a few neighboring surface atoms at the distance from the surface at which the electronic transitions occur. However, we shall not limit our model to the single dimension normal to the surface but shall also discuss the possible effects of surface atomicity.

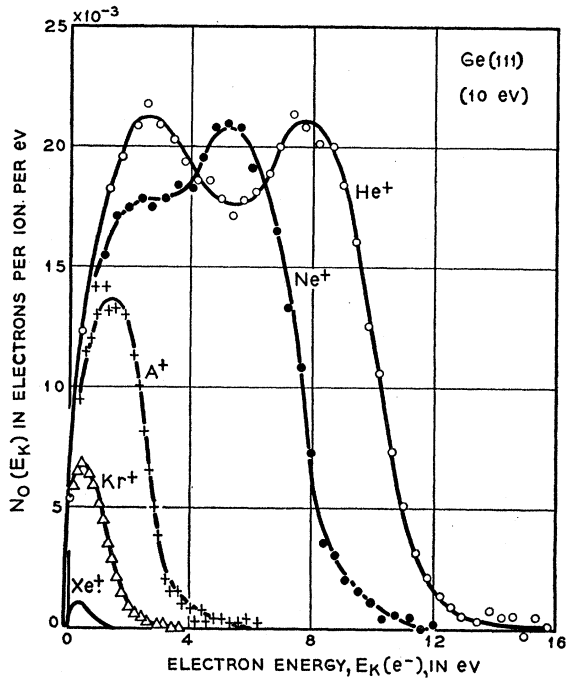

FIG. 1. Experimental kinetic energy distributions, $N_0(E_k)$, of electrons ejected from the Ge(111) face by 10-ev singly-charged ions of the noble gases (reference 1). The curves drawn through the experimental points represent smoothed experimental distributions.

Experimental results, in terms of which the present theory is developed, are those for the (111) face of germanium [Ge(111)].[1] In Fig. 1 are shown $N_0(E_k)$ distributions for noble gas ions of 10-ev incident kinetic energy. $N_0(E_k)$ is found to change in form as ion kinetic energy is increased. Experimental data for He^+ ions of five different kinetic energies are shown in Fig. 9. Since the area under an $N_0(E_k)$ curve is the total yield γ_i in electrons per ion, Fig. 9 indicates that for He^+ γ_i changes little with ion energy. This is also true for the other singly-charged noble gas ions. These experimental results for Ge(111) are much like those for Si(111) and Si(100) for which data are also available.[1] We shall see that the present theory can account for all the principal features of these experimental results.

III. THE ELECTRONIC TRANSITIONS

As has been shown previously for the refractory metals, we are dealing here with the release of electrons from the semiconductor in a two-electron, Auger-type process termed Auger neutralization.[5] The electronic transitions are shown in the energy level diagram of

[8] In this paper the term "ionization energy of an ion" is used to mean the first ionization energy of the parent atom from which the ion is formed and not to mean, as strict usage would demand, the first ionization energy of the ion itself, which is the second ionization energy of the parent atom.

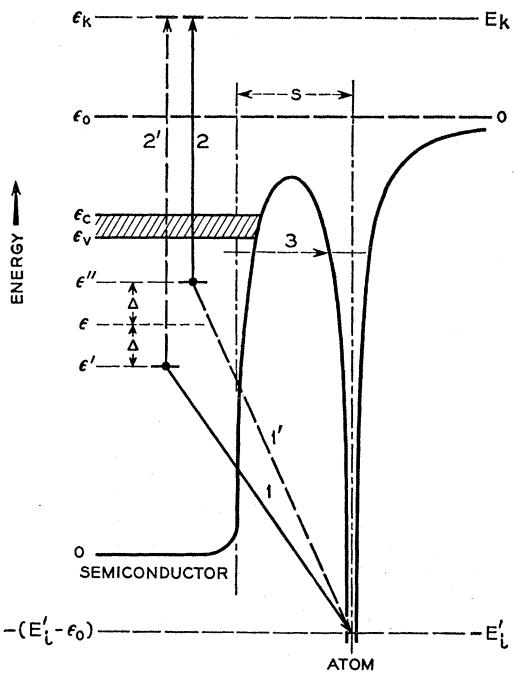

FIG. 2. Energy level diagram for an electron inside the semiconductor or in the field of the atomic core a distance s outside the solid surface. The two sets of Auger transitions shown (1, 2 and 1′, 2′) are obtained from each other by electron exchange. A resonance tunneling transition (3) to an excited atomic state is also shown. Energies inside the solid indicated to the left are taken to be zero at the bottom of the valence band. Energies outside the solid given by the scale at the right are zero at the vacuum level, the energy of a free electron at rest an infinite distance from both ion and solid.

Fig. 2. The two electrons involved have energies initially at ϵ' and ϵ'' in the valence band which extends from 0 to ϵ_v. One of these electrons tunnels into the ground state of the atom outside the solid. The second electron is simultaneously excited to the energy ϵ_k in the conduction band which extends from ϵ_c upward. As indicated in Fig. 2, two processes of this type are possible which are derived from one another by electron exchange. The impossibility of resonance tunneling to an excited state in the noble gases is pointed out in Sec. IV. Resonance tunneling to the ground state for Ne^+, A^+, Kr^+, and Xe^+ is discussed in Secs. IV and IX.

Equating the energy drop represented by transition 1 (or 1′) to the rise represented by transition 2 (or 2′) leads to the following statement of the conservation of energy:

$$\epsilon'+\epsilon''=2\epsilon=\epsilon_k+\epsilon_0-E_i'=E_k+2\epsilon_0-E_i'. \quad (1)$$

In Eq. (1) E_i' is an effective ionization energy for the atom near the solid surface which we do not expect to be the same as the free-space value E_i.

Since ϵ' and ϵ'' may lie anywhere in the valence band, we expect ϵ_k to be distributed over a band of energies whose limits may be calculated using Eq. (1). Maximum ϵ_k occurs for $\epsilon'=\epsilon''=\epsilon_v$ when both electrons lie initially at the top of the valence band. Thus,

$$(\epsilon_k)_{\max}=E_i'-\epsilon_0+2\epsilon_v. \quad (2)$$

Minimum ϵ_k is given by

$$\begin{aligned}(\epsilon_k)_{\min}&=E_i'-\epsilon_0 \quad \text{for} \quad E_i'-\epsilon_0>\epsilon_c\\ &=\epsilon_c \quad \text{for} \quad E_i'-\epsilon_0\leq\epsilon_c.\end{aligned} \quad (3)$$

$E_i'-\epsilon_0$ is calculated from (1) for $\epsilon'=\epsilon''=0$ when both electrons lie initially at the bottom of the valence band. However, any process for which $E_i'-\epsilon_0<\epsilon_c$ is impossible because it specifies a final state for the excited electron lying either in the forbidden gap, $\epsilon_v<\epsilon_k<\epsilon_c$, or in the already filled valence band, $0<\epsilon_k<\epsilon_v$.

The limits on kinetic energy outside the solid for those excited electrons which can surmount the surface barrier are:

$$(E_k)_{\max}=E_i'-2(\epsilon_0-\epsilon_v), \quad (4)$$

$$\begin{aligned}(E_k)_{\min}&=E_i'-2\epsilon_0 \quad \text{for} \quad E_i'-\epsilon_0>\epsilon_0\\ &=0 \quad \text{for} \quad E_i'-\epsilon_0\leq\epsilon_0.\end{aligned} \quad (5)$$

For $\epsilon_c<\epsilon_k<\epsilon_0$ the Auger neutralization process can occur but none of the excited electrons can leave the solid.

IV. BASIC ELEMENTS OF THE PHENOMENON

It is our purpose in this section to present the basic elements of the Auger neutralization process upon which the theoretical calculations of this paper are based. Equations introduced here appear again later in the numbered sequence of equations used in the calculations (Sec. V). A more detailed justification of the principal assumptions upon which the calculation rests is given later in the paper (Secs. XI–XV).

We wish to calculate the distribution in kinetic energy, $N_0(E_k)$ or $N_0(\epsilon_k)$, of electrons outside the semiconductor in terms of a number of parameters. The total electron yield, γ_i, is then the integral of $N_0(\epsilon_k)$ over all energies. $N_0(\epsilon_k)$ is related to the distribution in energy, $N_i(\epsilon_k)$, of all excited or Auger electrons inside the solid through a probability of electron escape or vacuum-level cutoff function, $P_e(\epsilon_k)$. Thus,

$$N_0(\epsilon_k)=N_i(\epsilon_k)P_e(\epsilon_k).$$

$P_e(\epsilon_k)$ specifies the fraction of electrons in $N_i(\epsilon_k)$ at any energy having sufficient momentum normal to the surface to escape over the surface barrier. It is calculable for a plane barrier and an $N_i(\epsilon_k)$ distribution which is isotropic in velocity at all ϵ_k. In general, $P_e(\epsilon_k)$ will depend upon the nature of the angular distribution of velocity in the $N_i(\epsilon_k)$ distribution and upon the shape of the surface barrier. Under all circumstances it is a function which rises from zero at the vacuum level, $\epsilon_k=\epsilon_0$, and approaches $\frac{1}{2}$ for very large ϵ_k if the probability of eventual release of an Auger electron moving initially away from the surface is small. N_0, N_i, and P_e functions for He^+ ions incident on the (111) face of germanium are shown in Fig. 3.

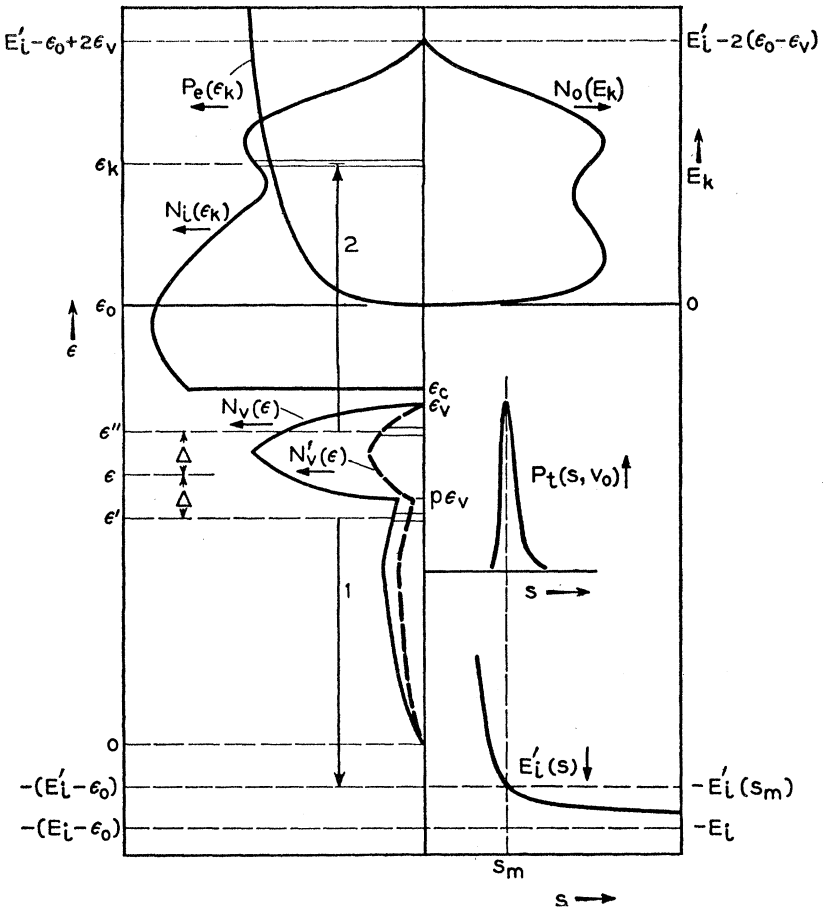

FIG. 3. Electron energy diagram like that of Fig. 2 on which are plotted the functional dependences of the theory introduced in the text in Sec. IV. The positive direction in which each function is plotted is indicated by an arrow alongside the function symbol. The functions plotted are those derived without energy broadening for the case of He^+ ions incident on the (111) face of germanium. However, they may also be taken as indicating schematically the types of functions in terms of which the theory is developed.

The $N_i(\epsilon_k)$ distribution, in turn, is expected to depend upon the variation of the matrix element of the Auger process with energy and upon the distribution, $N_v(\epsilon)$, of initial energy states in the valence band. In general, the matrix element may be expected to depend upon the initial energies ϵ' and ϵ'' directly and upon possible combinations of these energies such as their difference $\epsilon''-\epsilon'=2\Delta$. The direct dependence on initial energy may be accounted for by using an effective energy-level density function in the valence band, $N_v'(\epsilon)$, which is the product of the true density function $N_v(\epsilon)$ and a function $q(\epsilon)$ which specifies the relative variation of transition probability with energy. Thus,

$$N_v'(\epsilon)=q(\epsilon)N_v(\epsilon).$$

This equation states that a direct dependence of transition probability on energy is indistinguishable from a variation with energy of the number of electrons available to the Auger neutralization process. Smaller transition probability is equivalent to smaller effective number of electrons, and conversely. We shall see that this assumption is necessary and sufficient to account for the principal features of the experimental results. The forms of $N_v(\epsilon)$ and $N_v'(\epsilon)$ for germanium are shown in Fig. 3.

The dependence of $N_i(\epsilon_k)$ on $N_v'(\epsilon)$ may now be seen. Electrons populating the energy interval $d\epsilon$ at ϵ' and ϵ'' will produce excited electrons in the element $d\epsilon_k(=2d\epsilon)$ at ϵ_k. But so will electrons in intervals $d\epsilon$ at all pairs of energies ϵ' and ϵ'' which are symmetrically disposed with respect to the energy ϵ. Thus, we should expect $N_i(\epsilon_k)$ to be proportional to an integral over the product of effective state densities in the valence band, that is, proportional to the function $T(\epsilon_k)$ where $T(\epsilon)$ is given by

$$T(\epsilon)=\int N_v'(\epsilon-\Delta)N_v'(\epsilon+\Delta)d\Delta.$$

The integration stops when $\epsilon-\Delta=\epsilon''$ or $\epsilon+\Delta=\epsilon''$ reach the bottom or top of the valence band, respectively. The change of variable from ϵ to ϵ_k is that dictated by Eq. (1). $T(\epsilon)$ is the analog, for $N_v'(\epsilon)$, of the Auger transform defined by Lander[6] in terms of $N_v(\epsilon)$ for another Auger process possible in solids. It is noted here in passing that $N_i(\epsilon_k)$ should also depend upon the density of conduction band states, $N_c(\epsilon_k)$. $N_c(\epsilon_k)$ is assumed here to be a constant; its role in the theory will be discussed again later.

Because of the high probability of an Auger process relative to any radiative process,[3,7] we expect every ion

TABLE II. Semiconductor parameters used in this work.

	$\epsilon_0-\epsilon_v$ ev	$\epsilon_c-\epsilon_v$[d] ev	κ[e]
Ge(111)	4.8[a]	0.7	16
Si(111)	4.7[b]	1.1	12
Si(100)	5.1[c]	1.1	12

[a] This value is taken to be close to the value of the work function $\varphi=4.79$ ev measured by J. A. Dillon, Jr., and H. E. Farnsworth [J. Appl. Phys. **28**, 174 (1957)] on the grounds that the experimental surface, although clean, was strongly p type.

[b] J. A. Dillon, Jr., and H. E. Farnsworth [J. Appl. Phys. **29**, 1195 (1958)] quote φ for this face equal to 4.77 ev quenched, 4.67 ev annealed for one sample, 4.73 ev either quenched or annealed for a high resistivity floating zone sample. Eisinger [F. G. Allen, J. T. Eisinger, H. D. Hagstrum, and J. T. Law, J. Appl. Phys. **30**, 1563 (1959)] measured 4.77 ev after heating, which agrees well with the value of $\varphi=4.76$ ev for a cleaved surface measured by R. E. Simon [Bull. Am. Phys. Soc. **4**, 410 (1959)]. The value used here is again a little greater than the annealed value for a p-type surface.

[c] Dillon and Farnsworth (footnote b) give $\varphi=4.92$ ev quenched, 4.82 ev annealed. J. Eisinger as quoted by F. G. Allen [J. Phys. Chem. Solids **8**, 119 (1959)] measured a less certain value of 5.05 ev. In view of this uncertainty, the value 5.1 ev listed here is that found from fitting to the experimental data.

[d] These energy gap figures are rounded off to the nearest 0.1 ev from considerably more accurate data. See J. R. Haynes, M. Lax, and W. F. Flood, J. Phys. Chem. Solids **8**, 392 (1959). Also, G. C. MacFarlane, T. P. McLean, J. E. Quarrington, and V. Roberts, J. Phys. Chem. Solids **8**, 388 (1959); Phys. Rev. **111**, 1245 (1958).

[e] These are approximate figures of sufficient accuracy for present purposes based on more accurate measurements in the infrared and at lower frequencies. See H. B. Briggs, Phys. Rev. **77**, 287 (1950); W. C. Dunlap and R. L. Watters, Phys. Rev. **92**, 1396 (1953).

to be neutralized by Auger neutralization if direct resonance tunneling to the ground or excited states in the atom is impossible. Under these circumstances $N_i(\epsilon_k)$ is normalized to a total area of one electron per incident ion. Direct resonance tunneling to an excited level, illustrated by transition 3 in Fig. 2, appears to be impossible for the noble gas ions incident on silicon and germanium because all excited levels lie above the top of the valence band, at distances from the surface where these processes can occur. This may be seen by comparing $\epsilon_0-\epsilon_v$ values in Table II with the variation of excited levels with distance shown in Fig. 24 of reference 5. Tunneling into the excited state, if it occurs, will be followed by the Auger de-excitation process which produces Auger electrons distributed differently in energy from those produced by Auger neutralization.[5] It is thus essential to establish that resonance tunneling to an excited state cannot occur. Direct tunneling to the ground state is possible if the ground state lies at an energy above the bottom of the valence band, that is if $E_i'<\epsilon_0$. Its occurrence thus depends on the magnitudes of the ionization energy and the total width of the valence band and appears to be definitely impossible only for He^+ ions. This theory, in which $N_i(\epsilon_k)$ is normalized to one electron per ion, will overestimate the Auger yield if a fraction of the incident ions are neutralized by tunneling to the ground state (Sec. IX).

It is now necessary to introduce three further ideas, namely, (1) the dependence of transition probability on distance, s, of the atom from the surface, (2) the variation of ionization energy with distance of the atom from the surface, and (3) energy broadening of the N_i and N_0 distributions. All ions approaching the solid will not undergo Auger neutralization at the same distance from the surface. Transitions will be distributed in distance s according to a probability distribution we shall call $P_t(s,v_0)$ defined such that $P_t(s,v_0)ds$ is the probability that an ion moving with velocity v_0 will undergo neutralization in ds at s. $P_t(s,v_0)$ is a peak-shaped function like that shown in Fig. 3, passing through a maximum at $s=s_m$.

The ionization energy near the surface is less than the free-space value and varies with distance s. This results from the image and repulsive interactions between ion and solid and the repulsive interaction between neutralized atom and solid. Van der Waals interactions are so small relative to the energy discrimination of the experiment that they may be neglected. The form of the dependence of the effective ionization energy, E_i', on s is also shown in Fig. 3.

The combination of a P_t function of finite width and the variation of E_i' with s results in a variability of the energy level of the atomic ground state relative to the electronic energy levels in the solid. This introduces a broadening in energy ϵ_k of the N_i and N_0 distributions. Further energy broadening results from the Heisenberg uncertainty principle by virtue of the finite lifetimes in initial and final states of the Auger neutralization process.

V. STRUCTURE OF THE THEORETICAL CALCULATION

The preceding discussion of the basic elements of the theoretical problem suggests a procedure for calculating the $N_0(E_k)$ distribution. We start with a state density function, $N_v(\epsilon)$, derived from what is known about the general features of the population of the valence band in a diamond-type semiconductor.[9,10] Two of the four valence electrons are distributed over the entire valence bandwidth, $0<\epsilon<\epsilon_v$. These electrons vary in symmetry character from pure s at the bottom of the band to pure p at the top and account for the s electron and one of the three p electrons of the tetrahedral sp^3 hybridization of the valence band. The remaining two p electrons are distributed over narrower bands which are degenerate if we neglect spin-orbit coupling. These degenerate p bands lie at energies $p\epsilon_v<\epsilon<\epsilon_v$ at the top of the wider s-p band.

We assume a form of $N_v(\epsilon)$ involving the two parameters ϵ_v and p which is compounded of four parabolas N_1, N_2, N_3, and N_4. Thus,

$$N_v(\epsilon)=\sum_{n=1}^{4} N_n(\epsilon), \tag{6}$$

[9] F. Herman, Phys. Rev. **93**, 1214 (1954); Proc. Inst. Radio Engrs. **43**, 1703 (1955); Revs. Modern Phys. **30**, 102 (1958); J. Callaway, in *Solid State Physics*, edited by F. Seitz and D. Turnbull (Academic Press, Inc., New York, 1958), Vol. 7, p. 99.

[10] J. C. Phillips, Phys. Rev. **112**, 685 (1958).

where

$$N_1(\epsilon)=C_1\epsilon^{\frac{1}{2}}, \qquad 0\leq\epsilon\leq\epsilon_v/2, \tag{7}$$

$$N_2(\epsilon)=C_1(\epsilon_v-\epsilon)^{\frac{1}{2}}, \qquad \epsilon_v/2\leq\epsilon\leq\epsilon_v, \tag{8}$$

$$N_3(\epsilon)=C_2(\epsilon-p\epsilon_v)^{\frac{1}{2}}, \qquad p\epsilon_v\leq\epsilon\leq(1+p)\epsilon_v/2, \tag{9}$$

$$N_4(\epsilon)=C_2(\epsilon_v-\epsilon)^{\frac{1}{2}}, \qquad (1+p)\epsilon_v/2\leq\epsilon\leq\epsilon_v. \tag{10}$$

The constants C_1 and C_2 are determined by normalizing the area under each of the four parabolas to one electron. This yields:

$$C_1=\tfrac{3}{2}(\epsilon_v/2)^{-\frac{3}{2}}, \tag{11}$$

$$C_2=\tfrac{3}{2}[(1-p)\epsilon_v/2]^{-\frac{3}{2}}=C_1(1-p)^{-\frac{3}{2}}. \tag{12}$$

Values of p and ϵ_v determined from the fit to experiment for germanium are $p=0.73$ and $\epsilon_v=16$ ev, giving $C_1=0.0664$ and $C_2=0.473$. For silicon $p=0.68$, $\epsilon_v=16$ ev, giving $C_1=0.0664$ and $C_2=0.366$. The use of parabolas for the N_n functions means that we are assuming constant effective mass in each of the subbands.

The effective state density function $N_v'(\epsilon)$ is now defined in terms of $N_v(\epsilon)$ by the equations:

$$N_v'(\epsilon)=q(\epsilon)N_v(\epsilon)=\sum_{n=1}^{4}q_n(\epsilon)N_n(\epsilon) \quad \text{for} \quad 0\leq\epsilon\leq\epsilon_v$$
$$=0 \quad \text{for} \quad \epsilon\langle 0,\epsilon\rangle\epsilon_v. \tag{13}$$

As discussed above, this introduces a variation of transition probability with energy through the $q(\epsilon)$ function. We shall anticipate later discussion by stating here that this energy variation in all probability results from the variation of symmetry character of the valence electrons from s to p type through the band and the conclusion that a p-type valence electron has a lower transition probability than an s electron at the same energy. These statements lead to a $q(\epsilon)$ function of the form,

$$q_1(\epsilon)=q_2(\epsilon)=1-(1-r)(\epsilon/\epsilon_v), \tag{14}$$

$$q_3(\epsilon)=q_4(\epsilon)=r, \tag{15}$$

in which r, another parameter of the problem, is the ratio (≤ 1) of transition probability for a p to that for an s electron at the same energy. Equation (14) assumes a linear variation from s to p character through the s-p band specified by N_1 and N_2. Equation (15) reflects the fact that the degenerate bands given by N_3 and N_4 are completely p in character. At this point we may take (14) and (15) as giving an empirical form for $q(\epsilon)$ to be justified on the basis of the fit to experiment and later theoretical discussion. $N_v(\epsilon)$, $N_v'(\epsilon)$, and $q(\epsilon)$ are plotted for $r=0.3$ in Fig. 4.

The theory now proceeds with a calculation of the Auger transform $T(\epsilon)$ of the effective state density function. It is:

$$T(\epsilon)=\int_0^\infty N_v'(\epsilon-\Delta)N_v'(\epsilon+\Delta)d\Delta. \tag{16}$$

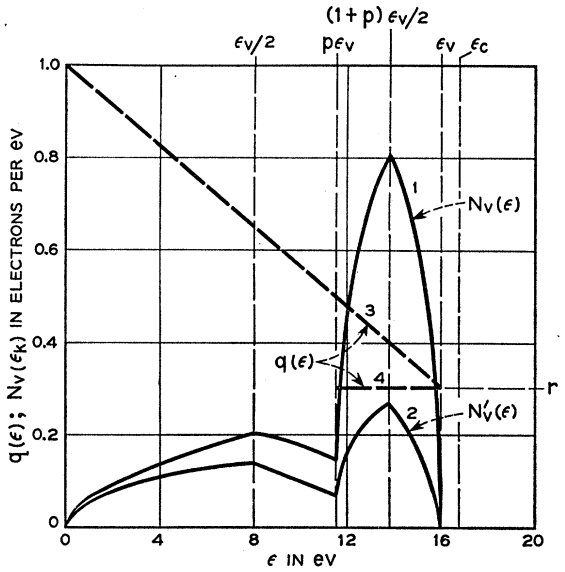

FIG. 4. The state density function $N_v(\epsilon)$ of Eqs. (6)–(10) (curve 1) and the effective state density function $N_v'(\epsilon)$ of Eq. (13) (curve 2) used in the theory for germanium. The $q(\epsilon)$ function is specified by $q_1=q_2$ of Eq. (14) (curve 3) and $q_3=q_4$ of Eq. (15) (curve 4). Parameters used are $\epsilon_v=16$ ev, $p=0.73$, $r=0.3$. Critical energies are indicated at the top of the diagram.

The details of computing this function for the assumed forms of $N_v(\epsilon)$ and $q(\epsilon)$ are given in the Appendix (Sec. XIX). By virtue of the definition of $N_v'(\epsilon)$ in Eq. (13) integration over Δ stops whenever either $\epsilon-\Delta$ or $\epsilon+\Delta$ leave the energy range of the valence band.

At this stage we introduce energy broadening by convoluting $T(\epsilon)$ with a broadening function $\varphi_\sigma(x)$ yielding the broadened Auger transform:

$$T_b(\epsilon)=\int_{-\infty}^{\infty}\varphi_\sigma(x)T(\epsilon+x)dx. \tag{17}$$

This procedure is introduced to account both for Heisenberg broadening and for broadening resulting from the variation of E_i' with s and the finite width of the P_i function on the s scale. In the present work a Gaussian broadening function,

$$\varphi_\sigma(x)=[1/\sigma(2\pi)^{\frac{1}{2}}]\exp(-x^2/2\sigma^2), \tag{18}$$

has been used. σ is the fourth parameter of the problem.

The simplification of using a single broadening function to account for the total effect of two quite different types of broadening is permissible for the slowest ions (10 ev) for which broadening effects are small. For faster ions where broadening becomes increasingly important, Gaussian broadening predicts the basic features of the experimental results but not the detailed form of the $N_0(\epsilon_k)$ distribution. Auger transforms $T(\epsilon)$ and $T_b(\epsilon)$ derived from the $N_v(\epsilon)$ and $N_v'(\epsilon)$ distributions of Fig. 4 are plotted in Fig. 5.

$N_i(\epsilon_k)$ is now taken to have the form of the broadened

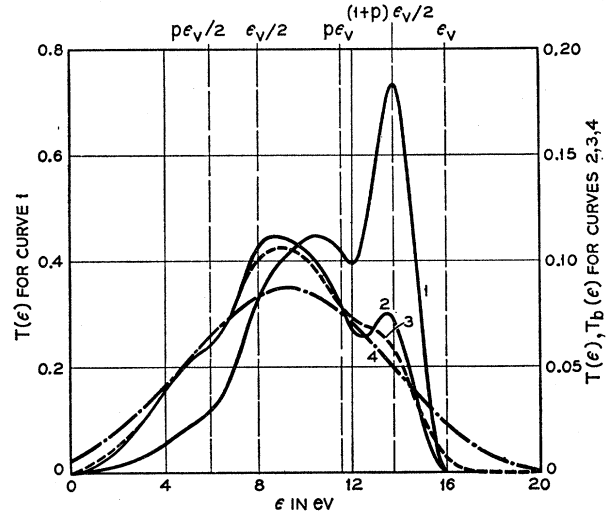

FIG. 5. $T(\epsilon)$ and $T_b(\epsilon)$ transforms derived from $N_v(\epsilon)$ and $N_v'(\epsilon)$ of Fig. 4 for germanium. Curve 1 is the unbroadened $T(\epsilon)$ from $N_v(\epsilon)$ (curve 1, Fig. 4, $r=1$). Curve 2 is the unbroadened $T(\epsilon)$ from $N_v'(\epsilon)$ (curve 2, Fig. 4, $r=0.3$). Curves 3 and 4 are broadened $T_b(\epsilon)$ functions from curve 2, Fig. 4, $r=0.3$. For curves 3 and 4 σ has the values 0.85 and 2.5 appropriate to the solution for 100- and 1000-ev ions, respectively. Critical energies are indicated at the top of the diagram.

Auger transform, $T_b(\epsilon)$. Thus,

$$N_i(\epsilon_k)=GT_b[\tfrac{1}{2}(\epsilon_k+\epsilon_0-E_i')], \tag{19}$$

in which G is a normalization factor. This step requires the change of variable from ϵ to ϵ_k according to Eq. (1). We may use a single value for E_i' in (1) since the effect of E_i' variation with s and finite P_t width have been accounted for in the broadening procedure. The value of E_i' required by fit to experiment should be close to $E_i'(s_m)$, the value at the maximum of the P_t function (Fig. 3). E_i' is the fifth parameter of the problem. ϵ_0 is known from the assumed value of ϵ_v and the photothreshold $(\epsilon_0-\epsilon_v)$ which has been measured for several crystallographic faces of germanium and silicon (Table II).

The $N_i(\epsilon_k)$ distribution is now normalized to an area of one electron per incident ion,

$$\int_{\epsilon_c}^{\infty} N_i(\epsilon_k)d\epsilon_k=1 \text{ electron per ion}, \tag{20}$$

yielding for the normalizing factor G of Eq. (19) the result:

$$1/G=\int_{\epsilon_c}^{\infty} T_b[\tfrac{1}{2}(\epsilon_k+\epsilon_0-E_i')]. \tag{21}$$

$N_i(\epsilon_k)$ distributions obtained from the $T(\epsilon)$ functions of Fig. 5 are plotted in Fig. 6. On this basis the theory gives an electron yield per ion neutralized in the Auger neutralization process. This result may be compared with that observed, as discussed above, only when Auger neutralization is the only neutralization process occurring.

Calculation of the external distribution $N_0(\epsilon_k)$ requires knowledge of the probability of electron escape over the surface barrier. For $N_i(\epsilon_k)$ isotropic in velocity relative to the surface normal and for a plane surface barrier of total height ϵ_0 above the bottom of the valence band, assuming that no electrons escape which are initially directed into the solid away from the surface, P_e is calculable and is given by[5]

$$\begin{aligned} P_e(\epsilon_k)&=\tfrac{1}{2}[1-(\epsilon_0/\epsilon_k)^{\frac{1}{2}}] \quad \text{for} \quad \epsilon_k>\epsilon_0 \\ &=0 \quad \text{for} \quad \epsilon_k<\epsilon_0. \end{aligned} \tag{22}$$

Equation (22) is plotted as curve 4 in Fig. 6. It is a function which starts from zero at $\epsilon_k=\epsilon_0$, the vacuum level, and approaches $\frac{1}{2}$ for large ϵ_k. We shall find that use of expression (22) permits the escape of too few electrons to account for the experimental electron yield. A one-parameter expression giving greater escape probabilities is that derived earlier[11]:

$$\begin{aligned} P_e(\epsilon_k)&=\tfrac{1}{2}[1-(\epsilon_0/\epsilon_k)^{\frac{1}{2}}]/[1-\alpha(\epsilon_0/\epsilon_k)^{\frac{1}{2}}] \text{ for } \epsilon_k>\epsilon_0 \\ &=0 \quad \text{for} \quad \epsilon_k<\epsilon_0. \end{aligned} \tag{23}$$

For $\alpha=0$ expression (23) reduces to (22); for $\alpha=1$ it gives $P_e=\frac{1}{2}$ at all energies. For $0<\alpha<1$, (23) lies higher than (22) but has the same general characteristics of rising from zero at $\epsilon_k=\epsilon_0$ and approaching $\frac{1}{2}$ for large

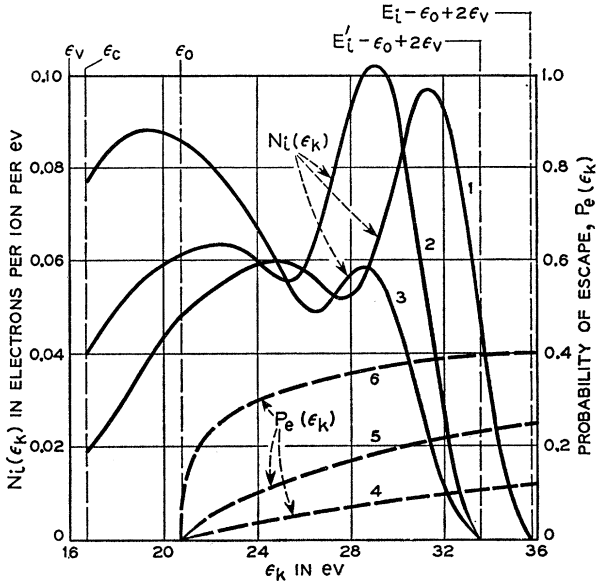

FIG. 6. Graph showing several $N_i(\epsilon_k)$ and $P_e(\epsilon_k)$ functions appropriate to the case of 10-ev He^+ ions on Ge(111). Curve 1 results from curve 1 of Fig. 5 with $E_i'=E_i=24.6$ ev, curve 2 from curve 1 of Fig. 5 with $E_i'=22.4$ ev, and curve 3 from curve 2 of Fig. 5 with $E_i'=22.4$ ev. Curve 4 is a plot of Eq. (22), curve 5 of Eq. (24) with $\alpha=0.78$, $\beta=1.0$, and curve 6 of Eq. (24) with $\alpha=0.25$, $\beta=1.0$. Critical energies are indicated at the top of the diagram.

[11] Equation (55) in reference 5.

TABLE III. Procedure for obtaining theoretical $N_0(E_k)$ distribution and γ_i.

Step	Equations	Parameters	Other quantities[a]
(1) Assume $N_v(\epsilon)$	(6)–(12)	ϵ_v, p	···
(2) Assume $q(\epsilon)$	(14), (15)	r	···
(3) Calculate $N_v'(\epsilon)$	(13)	···	···
(4) Calculate $T(\epsilon)$	(16)	···	···
(5) Assume $\varphi_\sigma(x)$	(18)	σ	···
(6) Calculate $T_b(\epsilon)$	(17)	···	···
(7) Calculate $N_i(\epsilon_k)$	(19)	E_i'	$(\epsilon_0-\epsilon_v)$
(8) Normalize $N_i(\epsilon_k)$	(20), (21)	···	$(\epsilon_c-\epsilon_v)$
(9) Assume $P_e(\epsilon_k)$	(22)–(24)	α, β	ϵ_0
(10) Calculate $N_0(E_k)$	(25)	···	···
(11) Calculate γ_i	(26)	···	ϵ_0

[a] See Table II.

ϵ_k. A somewhat more convenient P_e function, which has been used extensively in the present work, is the two-parameter expression:

$$P_e(\epsilon_k)=\tfrac{1}{2}[1-(\epsilon_0/\epsilon_k)^\beta]^\alpha \quad \text{for} \quad \epsilon_k>\epsilon_0 \\ =0 \quad \text{for} \quad \epsilon_k<\epsilon_0. \tag{24}$$

For $\alpha=1, \beta=\frac{1}{2}$ expression (24) reduces to (22); for $\alpha=0, \beta\neq 0$ it gives $P_e=\frac{1}{2}$ at all energies. For given $\beta\neq 0$, α in the range $1>\alpha>0$ determines the general magnitude of P_e and gives values higher than (22). The β parameter largely determines the curvature of the function as ϵ_k increases from ϵ_0. Curves 5 and 6 in Fig. 6 are plots of this function. Expression (24) also approaches $\frac{1}{2}$ at large ϵ_k for all positive α and β provided $\beta\neq 0$. $P_e(\epsilon_k)$ functions of Eqs. (23) and (24) are also plotted in Fig. 15.

In terms of one of the P_e functions introduced above we may now calculate $N_0(\epsilon_k)$ as

$$N_0(\epsilon_k)=N_i(\epsilon_k)P_e(\epsilon_k), \tag{25}$$

and the total electron yield γ_i as

$$\gamma_i=\int_{\epsilon_0}^{\infty} N_0(\epsilon_k)d\epsilon_k=\int_0^{\infty} N_0(E_k)dE_k. \tag{26}$$

The calculational procedure presented here has been programmed for an electronic computer (IBM 704 or 7090). The steps involved are summarized in convenient form in Table III. The program operates when supplied with the necessary parameters (column 3, Table III) and the other quantities involved (column 4, Table III), and prints out γ_i and the functions $N_0(\epsilon_k)$, $N_i(\epsilon_k)$, $T(\epsilon_k)$, and $T_b(\epsilon_k)$ for energy intervals in ϵ usually taken to be 0.25 ev.

VI. SIMPLEST SOLUTION AND STEP-BY-STEP REMOVAL OF ITS SIMPLIFICATIONS

We begin our attempt to fit the experimental results for He^+ ions shown in Fig. 1 by a calculation based on the simplest of assumptions. We shall: (1) neglect broadening making $\sigma=0$ in (18) and $T_b(\epsilon)=T(\epsilon)$ by (17); (2) use the $P_e(\epsilon_k)$ function of expression (22) which assumes an isotropic N_i distribution incident on a plane barrier; (3) use the free space ionization energy, that is, take $E_i'=E_i=24.6$ ev in (19); and (4) neglect any dependence of transition probability on energy, thus taking $r=1$ which gives $q(\epsilon)=1$ by (14) and (15) and $N_v'(\epsilon)=N_v(\epsilon)$ by (13). These assumptions eliminate steps 2, 3, 5, and 6 of Table III. In addition we shall use $\epsilon_v=16$ ev and $p=0.73$ for germanium which are the values found for the ultimate fit. We investigate variation of ϵ_v and p in Sec. VIII.

The $N_v(\epsilon)$ function used here is curve 1 of Fig. 4 which leads to the $T(\epsilon)$ function of curve 1 of Fig. 5. The $N_i(\epsilon_k)$ distribution is curve 1 of Fig. 6 and the assumed P_e function is curve 4 of Fig. 6. The resulting $N_0(\epsilon_k)$ distribution is curve 1 of Fig. 7 yielding a theoretical γ_i of 0.056. Comparing these results with the experimental γ_i of 0.196 and with the experimental points also shown in Fig. 7, we see that this first theoretical $N_0(\epsilon_k)$ is too small in magnitude, lies too high on the energy scale and has the wrong form. We shall now attempt to correct these deficiencies by a step-by-step removal of the simplifying assumptions.

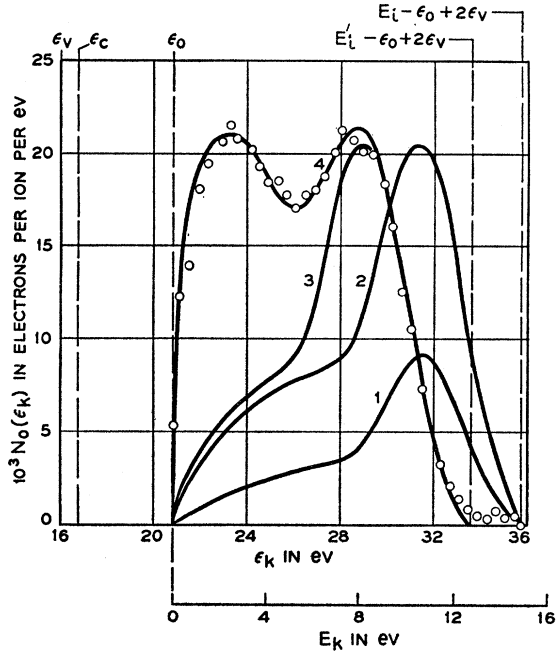

FIG. 7. Theoretical $N_0(\epsilon_k)$ distributions (full lines) for 10-ev He^+ ions on Ge(111) obtained with various simplifying assumptions. The experimental distribution is indicated by the points only. Curve 1 corresponds to curves 1, Figs. 4, 5, and 6 for the case of $r=1$, $E_i'=E_i=24.6$ ev and P_e of Eq. (22). Curve 2 corresponds to curves 1 of Figs. 4, 5, and 6 with $r=1$, $E_i'=24.6$ ev and P_e of Eq. (24) with $\alpha=0.78$, $\beta=1.0$. Curve 3 corresponds to curves 1, 1, 2 of Figs. 4, 5, 6, respectively, with $r=1$, $E_i'=22.4$ ev, and P_e of Eq. (24) with $\alpha=0.78$, $\beta=1.0$. Curve 4 corresponds to curves 2, 2, 3 of Figs. 4, 5, 6, respectively, with $r=0.3$, $E_i'=22.4$ ev, and P_e of Eq. (24) with $\alpha=0.25$, $\beta=1.0$. Critical energies are indicated at the top of the diagram and an E_k scale is given at the bottom.

TABLE IV. Parameters used in theoretical calculations.[a]

	Ion	K.E. ev	Target	$E_i'(s_m)$ ev	ϵ_v ev	ϵ_c ev	ϵ_0 ev	p	r	σ ev	α[b]	β[b]	γ_i
1	He^+	10	Ge(111)	**24.6**	16.0	16.7	20.8	0.73	**1.0**	0	...	...	0.056
2	He^+	10	Ge(111)	**24.6**	16.0	16.7	20.8	0.73	**1.0**	0	**0.78**	1.0	0.137
3	He^+	10	Ge(111)	**22.4**	16.0	16.7	20.8	0.73	**1.0**	0	**0.73**	1.0	0.120
4	He^+	10	Ge(111)	**22.4**	16.0	16.7	20.8	0.73	**0.3**	0	**0.25**	1.0	0.191
5	He^+	10	Ge(111)	**22.4**	16.0	16.7	20.8	0.73	0.30	**0.3**	0.248	1.0	0.198
6	He^+	33	Ge(111)	**22.2**	16.0	16.7	20.8	0.73	0.30	**0.5**	0.248	1.0	0.198
7	He^+	100	Ge(111)	**22.0**	16.0	16.7	20.8	0.73	0.30	**0.85**	0.248	1.0	0.196
8	He^+	333	Ge(111)	**21.5**	16.0	16.7	20.8	0.73	0.30	**1.5**	0.248	1.0	0.198
9	He^+	1000	Ge(111)	**20.5**	16.0	16.7	20.8	0.73	0.30	**2.5**	0.248	1.0	0.203
10	He^+	10	Ge(111)	22.0	**14.0**	14.7	18.8	**0.72**	0.32	0.3	0.300	1.0	0.194
11	He^+	10	Ge(111)	22.4	**14.0**	14.7	18.8	**0.69**	0.34	0.3	0.316	1.0	0.196
12	He^+	10	Ge(111)	22.4	**10.0**	10.7	14.8	**0.57**	0.4	0.3	0.318	0.25	0.181
13	He^+	10	Ge(111)	22.4	**10.0**	10.7	14.8	**0.68**	0.4	0.3	0.318	0.25	0.174
14	Ne^+	10	Ge(111)	**19.8**	16.0	16.7	20.8	0.73	**0.30**	0.3	0.248	1.0	0.166
15	Ne^+	10	Ge(111)	**19.8**	16.0	16.7	20.8	0.73	**0.25**	0.3	0.290	1.0	0.145
16	A^+	10	Ge(111)	**14.2**	16.0	16.7	20.8	0.73	0.30	0.3	0.248	1.0	0.079
17	Kr^+	10	Ge(111)	**12.4**	16.0	16.7	20.8	0.73	0.30	0.3	0.248	1.0	0.825
18	He^+	10	Si(111)	22.6	16.0	17.1	20.7	**0.68**	0.34	0.3	0.935	...	0.191
19	He^+	10	Si(100)	22.6	16.0	17.1	21.1	**0.68**	0.34	0.3	0.935	...	0.127

[a] Parameters of particular interest in any sequence of runs are indicated in bold-faced type.
[b] The $P_e(\epsilon_k)$ expression for any line of the table is that of Eq. (22) if neither α nor β is specified, Eq. (23) if α only is given, and Eq. (24) if both α and β are given.

The only way to increase substantially the magnitude of $N_0(\epsilon_k)$ above that of curve 1 of Fig. 7 while meeting other requirements is to increase the probability of escape. If we replace Eq. (22) for P_e by Eq. (24) with $\alpha=0.78, \beta=1.0$ P_e has the form of curve 5 of Fig. 6. Keeping all other parameters at the values initially chosen, we obtain for $N_0(\epsilon_k)$ curve 2 of Fig. 7, the product of curves 1 and 5 of Fig. 6. The values of α and β used were chosen to give a height of the $N_0(E_k)$ function approximately equal to that of the experimental one.

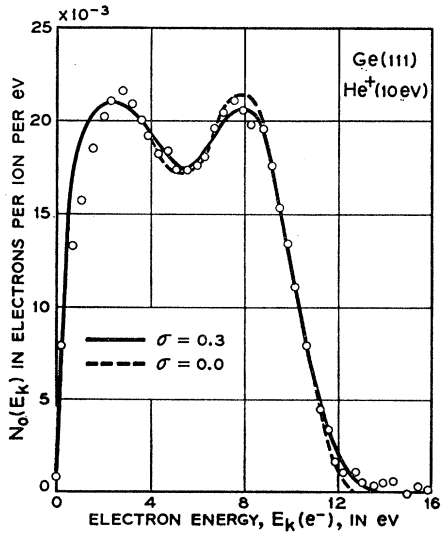

FIG. 8. Theoretical $N_0(E_k)$ distributions (lines) compared with the experimental distribution (points only) for 10-ev He^+ ions incident on Ge(111). The full curve is for a small amount of energy broadening ($\sigma=0.3$), the dashed curve for no broadening ($\sigma=0$). Parameters used in the calculation of these curves are listed in lines 5 and 4 of Table IV, respectively.

We now proceed to bring the high-energy limit of $N_0(E_k)$ into agreement with the experimental data. The controlling step here is the change of variable involved in calculating $N_i(\epsilon_k)$ from $T(\epsilon)$ (step 7 of Table III). Equation (4) indicates that $(E_k)_{\max}$ is governed by both E_i' and the photothreshold $(\epsilon_0-\epsilon_v)$. Since the latter is known for germanium, the only parameter at our disposal for shifting the high-energy limit of N_0 is E_i'. Our choice of $E_i'=E_i=24.6$ ev for He^+ is clearly too high. If $E_i'=22.4$ ev, we obtain curve 2 of Fig. 6 for $N_i(\epsilon_k)$. Again using curve 5 of Fig. 6 for P_e, the $N_0(\epsilon_k)$ of curve 3 of Fig. 7 results.

Curve 3 of Fig. 7 still represents a wide departure from the experimental distribution. The theory at this point produces proportionately far too many electrons near the top of the distribution which are those coming from near the top of the valence band. We need a variation of transition probability with energy through the valence band which discriminates against electrons lying high in the band. This is provided by the $q(\epsilon)$ function given in Eqs. (14) and (15) and introduced into the theory as indicated in Eq. (13). It is found that a value of $r=0.3$ is necessary to fit the data. This gives curve 2 of Fig. 4 for $N_v(\epsilon)$ with $q(\epsilon)$ given by curves 3 and 4. The corresponding $T(\epsilon)$ and $N_i(\epsilon_k)$ functions are curve 2 of Fig. 5 and curve 3 of Fig. 6, respectively, keeping $E_i'=22.4$ ev. It is now necessary to increase the magnitude of $P_e(\epsilon_k)$ further to obtain an N_0 function of the experimental magnitude. Curve 4 of Fig. 7, in good agreement with the experimental points, is obtained for the P_e of curve 6 of Fig. 6 for which $\alpha=0.25, \beta=1.0$.

It should be observed that the steps required to go from curve 1 to curve 4 in Fig. 7 are unique. The parameters involved (lines 1–4, Table IV) affect $N_0(E_k)$ in what might be termed an orthogonal manner. In

curve 4 of Fig. 7 we have achieved a quite respectable fit of theory to experiment without energy broadening. We shall not be surprised to find that for 10-ev ions broadening effects are small. However, the theoretical solution is so close to correct for $\sigma=0$ and the solution is so insensitive to relatively large changes of σ in the range $0<\sigma<0.5$ that one cannot accurately determine σ for 10-ev ions based on the 10-ev results alone. Fitting theory to experiment at higher ion kinetic energies, where broadening is important (Sec. VII) gives by extrapolation $\sigma\sim0.3$ ev for 10-ev He^+ ions. In Fig. 8 theoretical curves for $\sigma=0$ and $\sigma=0.3$ are shown and compared again with the experimental points.

VII. ENERGY BROADENING AND THE VARIATION WITH ION KINETIC ENERGY

Energy broadening, although relatively unimportant for 10-ev ions, becomes increasingly important as ion kinetic energy is increased. This fact enables one to study more closely the nature of energy broadening in the Auger neutralization process. In Fig. 9 are shown experimental N_0 distributions for He^+ ions of five different kinetic energies incident on Ge(111). There are two distinguishable effects to be seen in these curves. As ion energy increases the distribution is increasingly broadened as is evidenced by the formation of a longer and longer tail at high energies and the gradual disappearance of the higher energy peak of the two present in the 10-ev curve. The second effect is the shift of the higher energy peak to lower energies indicating a reduction of E_i' as ion energy increases.

An attempt has been made to predict these changes in $N_0(E_k)$ using the calculational procedures of Sec. V and Table III starting with the parameters which fit the 10-ev curve and changing E_i' and σ only as ion energy is increased. The results are shown in Fig. 10. The general features of the experimental curves have certainly been reproduced by theory. The detailed fit becomes poorer as ion energy increases, however, most likely as a result of the use of Gaussian broadening. The values of the E_i' parameter were chosen so that the theoretical distributions all cross each other at $E_k(e^-)\sim10.2$ ev as do the experimental ones. The $T_b(\epsilon)$ functions for the 100-ev ($\sigma=0.85$) and 1000-ev ($\sigma=2.5$) kinetic energies are curves 3 and 4 of Fig. 5, respectively.

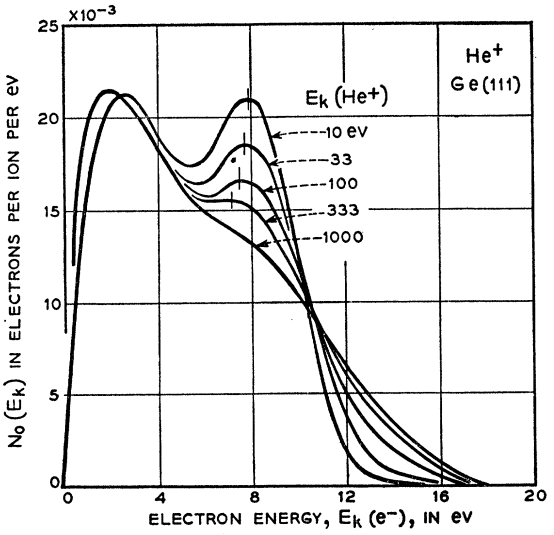

FIG. 9. Experimental $N_0(E_k)$ distributions for He^+ ions incident on Ge(111) having the kinetic energies indicated (reference 1). These curves are smoothed distributions like those of Fig. 1 drawn through data points which are not shown.

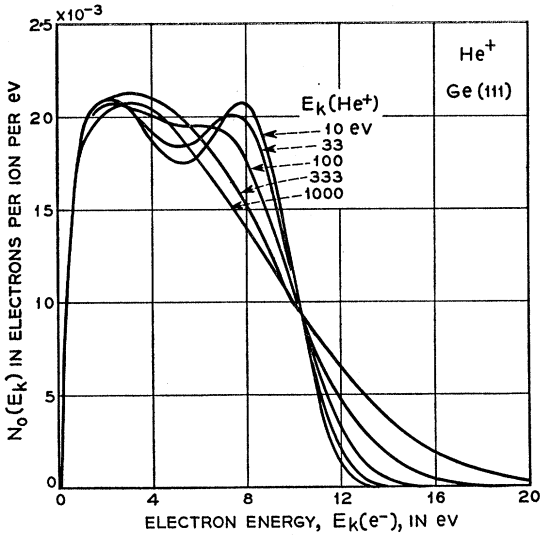

FIG. 10. Theoretical $N_0(E_k)$ distributions to be compared with the experimental ones of Fig. 9. Parameters used in the calculations are listed in lines 5–9 of Table IV.

VIII. UNIQUENESS OF THE FIT OF THEORY TO EXPERIMENT

We must now look into the question of uniqueness of the theoretical solutions. We have already noted the uniqueness of the steps required to go from curve 1 to curve 4 in Fig. 7. In these calculations, however, values for ϵ_v and p were used which were those of the ultimate best fit. We shall now investigate the uniqueness of the solution for He^+ (10 ev) on Ge(111) with respect to variation of each of the parameters of the problem. This will also indicate the probable error with which each parameter is obtained.

E_i', $(\epsilon_0-\epsilon_v)$. These parameters enter the theory in the combination $E_i'-2(\epsilon_0-\epsilon_v)$ and determine by Eq. (4) the upper energy limit of the $N_0(E_k)$ distribution. Even though the photothreshold, $(\epsilon_0-\epsilon_v)$, is known for Ge(111) (Table II), the effects of small variations in both E_i' and $(\epsilon_0-\epsilon_v)$ are shown in Fig. 11.

p. Figure 12 shows that near the true solution variation of p affects only the width of the higher energy peak of $N_0(E_k)$.

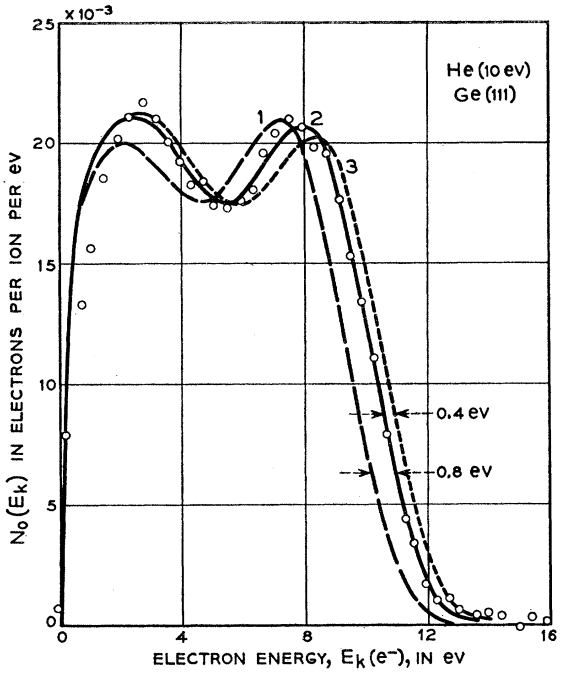

FIG. 11. Effect of variation of the parameters E_i' and $(\epsilon_0-\epsilon_v)$ on the theoretical $N_0(E_k)$ for 10-ev He^+ ions on Ge(111). Curve 2 is the best fit of line 5, Table IV with $E_i'=22.4$ ev and $(\epsilon_0-\epsilon_v)=4.8$ ev (Table II). The other curves have the same parameters except that $(\epsilon_0-\epsilon_v)=5.2$ ev for curve 1 and $E_i'=22.8$ ev for curve 3. Note that increase in E_i' by 0.4 ev increases the upper energy limit by the same amount whereas increase in $(\epsilon_0-\epsilon_v)$ by 0.4 ev decreases this limit by twice 0.4 ev.

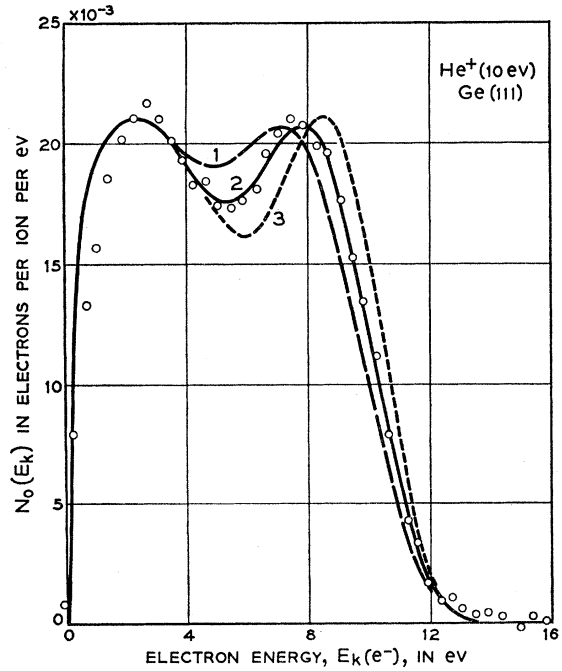

FIG. 12. Effect of variation of the parameter p. Curve 2 is again the best fit of line 5, Table IV with $p=0.73$. For curves 1 and 3, p has the values 0.70 and 0.76, respectively, all other parameters remaining unchanged.

r. Figure 13 shows that small changes in r affect only the height of the higher energy peak of $N_0(E_k)$.

$P_e(\epsilon_k)$. Variation of the level of $P_e(\epsilon_k)$ by variation of the parameter α in either of Eqs. (23) or (24) affects the height of the whole $N_0(E_k)$ distribution as shown in Fig. 14. Changes in curvature of the $P_e(\epsilon_k)$ function keeping the general level constant (Fig. 15) produce the changes in $N_0(E_k)$ shown in Fig. 16. Such changes in the curvature of $P_e(\epsilon_k)$ cannot be distinguished in this theory from other gentle variations with energy introduced by minor modifications in the forms of the $q(\epsilon)$ and $N_c(\epsilon_k)$ functions. $q(\epsilon)$ most likely is not strictly linear as assumed in Eqs. (14) and (15), and $N_c(\epsilon_k)$ is not constant as assumed above. This coupling among $q(\epsilon)$, $N_c(\epsilon_k)$, and $P_e(\epsilon_k)$ in no way alters the principal conclusions of the fit (Sec. X). Only relatively minor changes in any one of these functions may be compensated for by reasonable changes in the others.

ϵ_v. It was found early in this work that for both germanium and silicon serious difficulties were met when the attempt was made to fit the experimental data for values of ϵ_v much below 16 ev. Attempts to fit the 10-ev He^+ data on Ge(111) for $\epsilon_v=14$ and 10 ev are shown in Figs. 17 and 18, respectively. One concludes, on the basis of extensive investigations of this type, that ϵ_v must lie in the range 14–16 ev for both Ge and Si. It is recognized that this result is more

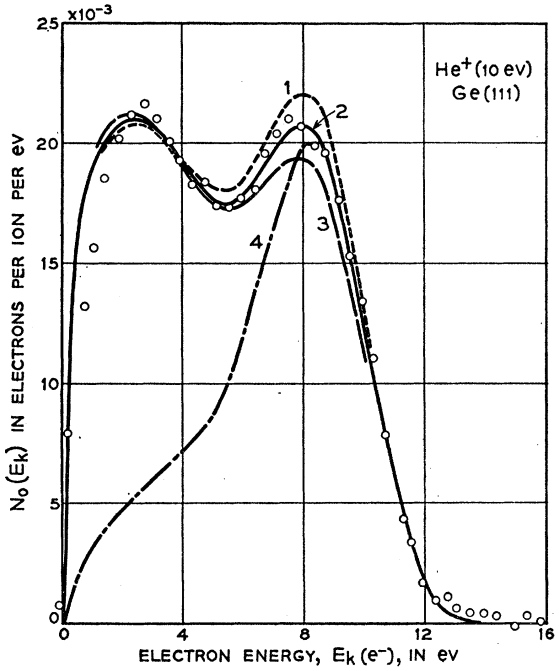

FIG. 13. Effect of variation of the parameter r. The best fit of line 5, Table IV with $r=0.30$ is shown by curve 2. In curves 1 and 3, r has the values 0.33 and 0.27, respectively, all other parameters unchanged. Curve 4 shows the result of choosing $r=1$ with the parameters of P_e (line 3, Table IV) chosen to give approximately the correct height for the higher energy peak.

sensitive to the form chosen for $N_v(\epsilon)$ than are the values obtained for the other parameters (see Sec. XVI).

σ. It was shown in Secs. VI and VII that the fit at 10 ev is insensitive to σ since broadening is small and that the best value for 10-ev ions is determined by extrapolation from higher ion energies where $N_0(\epsilon_k)$ is more sensitive to σ. A study of the accuracy with which broadening can be specified at higher ion energies must await the use of a broadening function which more accurately reproduces $N_0(E_k)$ at these ion energies than does the Gaussian function. Possible error in σ for higher ion energies will not change the conclusion that σ is of the order of 0.3 for 10-ev ions.

From the foregoing we see that uniqueness of the main features of the solution is maintained when the variation of all parameters is considered. From a study of the graphs showing the effects of varying the parameters individually, one can determine that a change of one parameter cannot be compensated for by any combination of changes in the other parameters. This uniqueness allows latitude for only minor variations in the functions $q(\epsilon)$, $N_v(\epsilon)$, $N_c(\epsilon_k)$, and $P_e(\epsilon_k)$, as has been mentioned above and will be discussed again in Sec. XV.

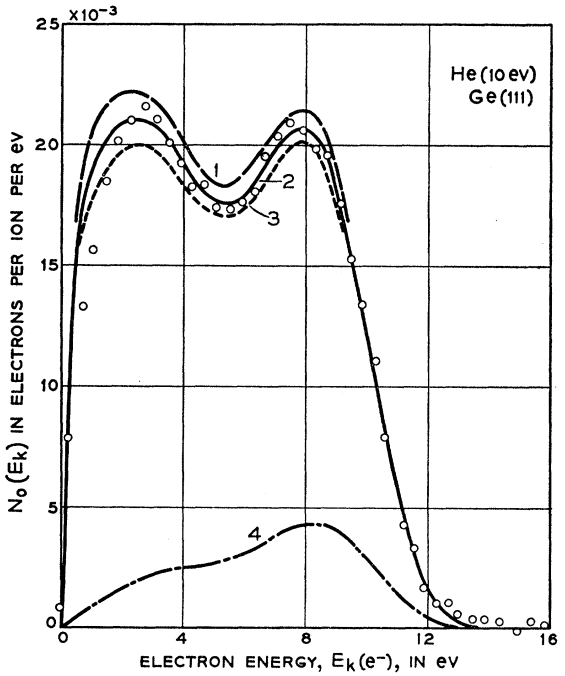

FIG. 14. Effect of variation of the α parameter in the two-parameter formula for $P_e(\epsilon_k)$ [Eq. (24)]. Curve 2 is again the best fit of line 5, Table IV with $\alpha=0.248$. For curves 1 and 3, α is 0.224 and 0.272, respectively, all other parameters remaining unchanged. Curve 4 is for $P_e(\epsilon_k)$ [Eq. (22)] appropriate to an isotropic velocity distribution of excited electrons incident on a plane barrier. Parameters for curve 4 are given in line 1 of Table IV.

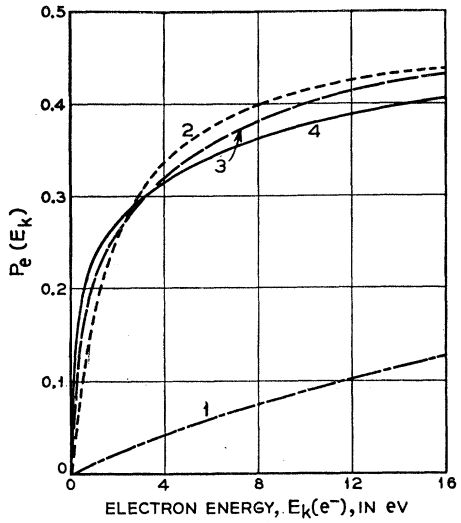

FIG. 15. Plots of several $P_e(\epsilon_k)$ functions. Curve 1 is for the isotropic $N_i(\epsilon_k)$ distribution on a plane barrier [Eq. (22)]. Curve 2 is a plot of Eq. (23) with $\alpha=0.956$. Curves 3 and 4 are plots of Eq. (24) with $\alpha=0.248$, $\beta=1.0$ and $\alpha=0.366$, $\beta=2.0$, respectively. Curves 2, 3, and 4 show P_e functions of about the same level but of different curvature.

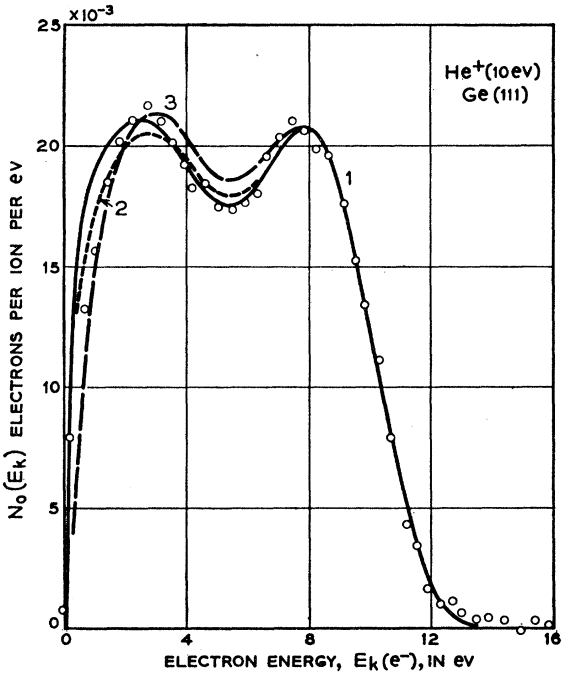

FIG. 16. Variation of the theoretical $N_0(E_k)$ distributions for He^+ (10 ev) on Ge(111) caused by the use of $P_e(\epsilon_k)$ functions of different curvature. Curve 1 is the best fit (line 5, Table IV) using Eq. (24) with $\alpha=0.248$, $\beta=1.0$ (curve 4, Fig. 15). For curve 2, Eq. (24) was used with $\alpha=0.366$, $\beta=2.0$ (curve 3, Fig. 15). For curve 3, Eq. (23) was used with $\alpha=0.956$ (curve 2, Fig. 15). All other parameters were the same for the three curves except for r which was varied from the 0.3 value for curve 1 to 0.28 and 0.26 for curves 2 and 3, respectively, in order to compensate for the change in slope of the P_e functions used.

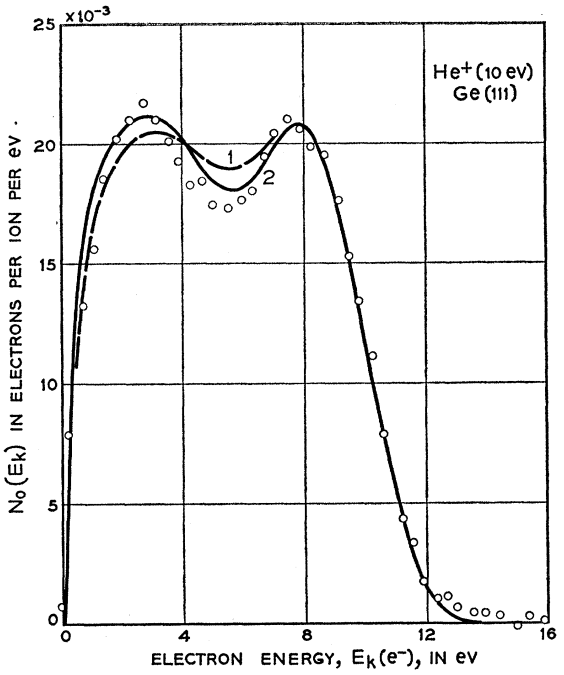

FIG. 17. Two attempts to fit the experimental $N_0(E_k)$ distribution for He^+ (10 ev) on Ge(111) using a total bandwidth, ϵ_v, of 14 ev. The parameters used in curves 1 and 2 are listed in lines 10 and 11 of Table IV, respectively. It is impossible to reproduce the minimum of the experimental distribution both as to depth and position under these circumstances.

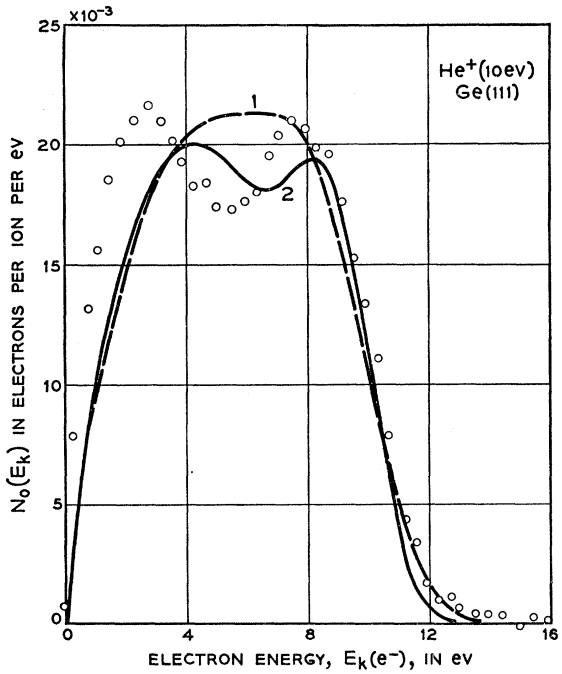

FIG. 18. Two attempts to fit the experimental $N_0(E_k)$ distribution for He^+ (10 ev) on Ge(111) using $\epsilon_v=10$ ev. Parameters for curves 1 and 2 are listed in lines 12 and 13 of Table IV. Note the impossibility of producing a minimum in the curve at the correct energy position and of the proper depth.

IX. SOLUTIONS FOR OTHER NOBLE GAS IONS AND FOR SILICON

Theoretical $N_0(E_k)$ distributions have also been calculated for 10-ev Ne^+, A^+, and Kr^+ ions incident on Ge(111) in an attempt to fit the experimental data of Fig. 1. The simplest procedure is to use all the parameters found for 10-ev He^+ (line 5, Table IV) except E_i' which is determined for each ion so as to reproduce the experimental high-energy limit of $N_0(E_k)$. The resulting theoretical $N_0(E_k)$ distributions for Ne^+ and Kr^+ are shown in Figs. 19 and 20, respectively. Parameters for Ne^+, A^+, and Kr^+ are given in lines 14–17 of Table IV.

The theoretical $N_0(E_k)$ lies increasingly higher than the experimental data through the sequence Ne^+, A^+, Kr^+. The factor by which the theoretical curve, and hence theoretical total electron yield, must be multiplied to bring it down to the experimental data is 0.87 for Ne^+, 0.45 for A^+, and 0.36 for Kr^+. Neither experiment nor theory is very reliable for Xe^+. It is believed that the principal reason for this increasing disparity between theory and experiment as E_i is decreased is an increasing resonance tunneling into the ground state. If a fraction W of incident ions is resonance neutralized to the ground state, we should use $\int_{\epsilon_c}^{\infty} N_i(\epsilon_k)d\epsilon_k = 1-W$ in place of Eq. (20). The factors 0.87, 0.45, and 0.36 by which the theoretical yield exceeds the experimental for

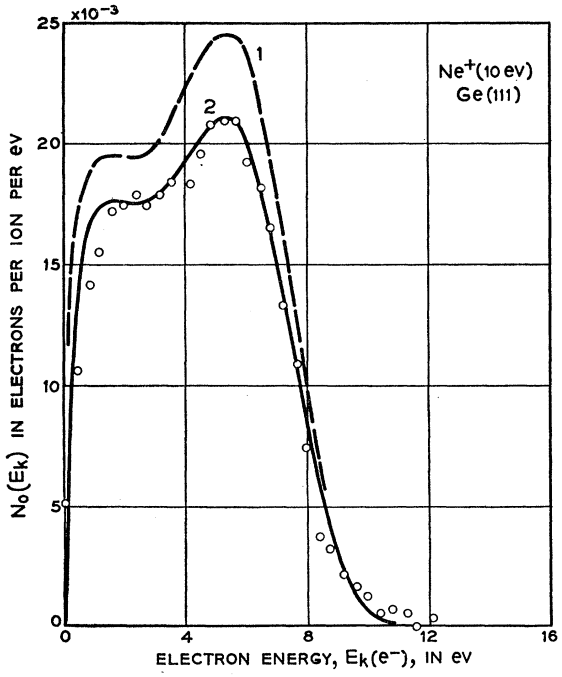

FIG. 19. Attempts to fit theoretically the experimental $N_0(E_k)$ distribution for Ne^+ (10 ev) on Ge(111). Points are experimental. For curve 1 (line 14, Table IV) only E_i' was changed from that used for the He^+ curves ($\sigma=0.3$) in Fig. 8 (line 5, Table IV). For curve 2, in addition to the change in E_i', r and α were changed slightly from the He^+ values (line 15, Table IV). Curve 2 is quite close to the curve one obtains by multiplying curve 1 by 0.87.

Ne^+, A^+, and Kr^+ are then to be interpreted as $1-W$ for these ions. The fact that W increases with decreasing E_i', as is expected for resonance tunneling, lends credence to this explanation. It is true that as E_i' decreases the theoretical fit becomes more sensitive to the detailed forms of $N_v'(\epsilon)$, $\varphi_\sigma(x)$, $P_e(\epsilon_k)$, and to the exact value of E_v'. One cannot decrease W to zero for A^+ and Kr^+ by changes in the theoretical parameters which are at all reasonable for He^+ and Ne^+. Relatively minor changes in the parameters for the Ne^+ fit will reduce W to zero for Ne^+ as is indicated in Fig. 19. If W is in fact greater than zero for Ne^+, it means that $\epsilon_0 > E_i'(Ne^+) = 19.8$ ev (line 15, Table IV). This sets a lower bound for ϵ_v of $E_i' - (\epsilon_0 - \epsilon_v) = 19.8 - 4.8 = 15$ ev, since $\epsilon_0 - \epsilon_v = 4.8$ ev is known (Table II). If resonance tunneling occurs first for A^+, then the lower bound on ϵ_v is $E_i'(A^+) - (\epsilon_0 - \epsilon_v) = 9.4$ ev using the data of line 16 of Table IV.

Theoretical calculations have been made of $N_0(E_k)$ and γ_i for He^+, Ne^+, A^+, and Kr^+ incident on the (111) and (100) faces of silicon for which experimental data are also available.[1] The theory works as well here as for germanium. Theoretical $N_0(E_k)$ curves for 10-ev He^+ on Si(111) and Si(100) are shown in Fig. 21 where they are compared with experimental data. E_i' is within 0.2 ev of that found for Ge(111). The level of $P_e(\epsilon_k)$ is approximately the same as that required for Ge(111). Little difference in ϵ_v is found between Si and Ge, but p is smaller by a significant amount for Si predicting a somewhat wider degenerate p band. It is for this reason that the minimum near 5 ev in $N_0(E_k)$ for 10-ev He^+ on Ge(111) is not nearly as well developed in the corresponding $N_0(E_k)$ for Si(111).

Theoretical $N_0(E_k)$ curves for He^+ ions of various kinetic energies incident on Si(100) have been calculated also. The same degree of agreement with experiment was found, as is reported here for He^+ on Ge(111), in Figs. 9 and 10. These results bolster one's confidence in the general credibility of the theoretical model.

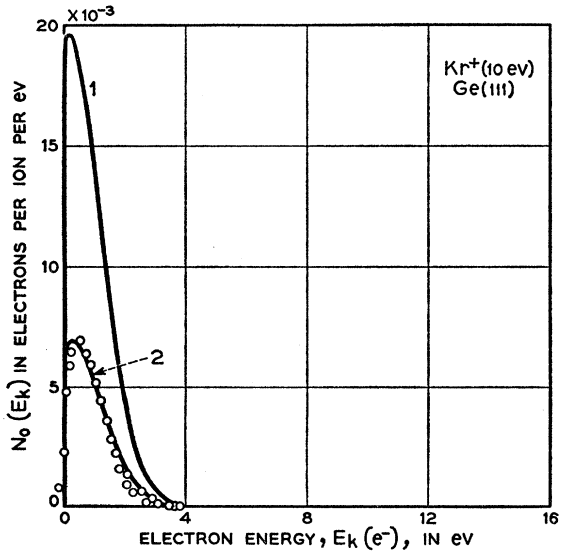

FIG. 20. Comparison of theory and experiment for $N_0(E_k)$ from Kr^+ (10 ev) on Ge(111). Points are experimental. Curve 1 is theoretical for the parameters of line 17, Table IV, and curve 2 is curve 1 multiplied by 0.36.

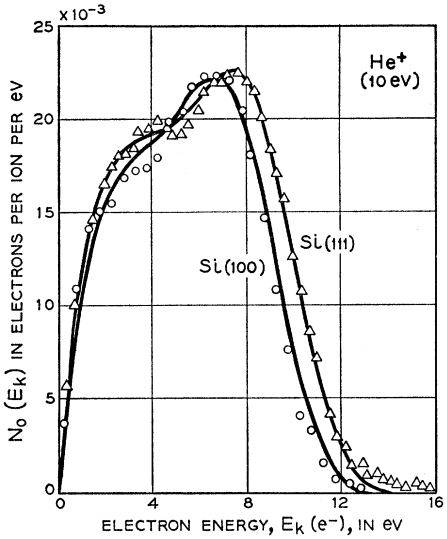

FIG. 21. Theoretical $N_0(E_k)$ distributions compared with the experimental points for 10-ev He^+ on the (111) and (100) faces of Si. Parameters for the Si(111) curve are given in line 18 of Table IV. The same parameters were used for the Si(100) curve except for ϵ_0 which is determined by the appropriate change in photothreshold $\epsilon_0 - \epsilon_v$ (see Table II and line 19 of Table IV).

X. CONCLUSIONS OF THE FIT OF THEORY TO EXPERIMENT

In what has preceded in this paper we have discussed the basic elements of the Auger neutralization process and devised a calculational procedure for fitting the experimental data. It has been possible to find a unique solution which reproduces all the principal features of the experimental results. The requirements of the fit have forced upon us four basic conclusions concerning the Auger neutralization process. These are:

(1) The relative Auger transition probability represented by the function $q(\epsilon)$ decreases with energy through the valence band having a value at the top of the band about 0.3 that at the bottom ($r = 0.3$).

(2) The effective ionization energy, E_i', in the Auger process is less than the free-space value, E_i, and decreases with increasing ion velocity. For He^+ the E_i' values in lines 5–9 of Table IV are represented with reasonable accuracy by the expression:

$$E_i - E_i' \cong 2 + 0.06(E_k + 2)^{\frac{1}{2}}, \tag{27}$$

in which E_k is the ion's incident kinetic energy at $s = \infty$ and E_i, E_i', and E_k are in ev. $E_i - E_i'$ obtained from the fit to experiment is compared with the predictions of Eq. (27) in Table V.

(3) Energy broadening is small for the slowest ions (10 ev) but must be included for faster ions (<1000 ev). The parameter σ in the Gaussian broadening function

TABLE V. Comparison of E_i-E_i' and σ obtained from the fit of theory to experiment and the empirical formulas [He^+ on Ge(111)].

$E_k(He^+)$	E_i-E_i' (ev) From the fit[a]	E_i-E_i' (ev) $2+0.06\times(E_k+2)^{\frac{1}{2}}$	σ (ev) From the fit[a]	σ (ev) $0.083\times(E_k+2)^{\frac{1}{2}}$
10	2.2	2.21	(0.3)	0.29
33	2.4	2.36	0.50	0.49
100	2.6	2.61	0.85	0.84
333	3.1	3.10	1.5	1.52
1000	4.1	3.91	2.5	2.64

[a] Lines 5–9 of Table IV.

used is found to increase approximately linearly with ion velocity at the distance from the surface where Auger neutralization takes place. For He^+ σ values in lines 5–9 of Table IV are given with good accuracy by the expression:

$$\sigma\cong 0.083(E_k+2)^{\frac{1}{2}}, \tag{28}$$

in which again E_k is the ion's kinetic energy at $s=\infty$ and both σ and E_k are in ev. Table V also includes a comparison of σ values from the fit to experiment and those derived from Eq. (28).

(4) The probability of electron escape in the range of external electron energy involved here (0–12 ev) is several times greater in magnitude than that predicted for an isotropic distribution of internal Auger electrons incident on a plane barrier. This ratio is a function of energy and is best seen by comparing the levels of curves 2, 3, and 4 with that of curve 1 in Fig. 15.

It is our purpose in the next sections of the paper to discuss these conclusions in the light of theory. Our purpose is to get at the basic significance of these conclusions rather than to attempt to derive them rigorously from first principles.

XI. TRANSITION RATE AND BASIC PROBABILITY DISTRIBUTIONS

The transition rate, r_t, for an elemental Auger transition (Fig. 3) is given by time-dependent perturbation theory using the method of variation of constants as

$$r_t(\epsilon',\epsilon'',\theta,\varphi,s)=(2\pi/\hbar)\,|H_{fi}|^2 N_c(\epsilon_k)d\Omega. \tag{29}$$

The rate r_t is expected to be a function of initial electron energies, ϵ' and ϵ'', of direction of the excited electron's velocity, θ and φ, and of distance, s, between ion and surface when the process occurs. In Eq. (29), H_{fi} is the matrix element, and $N_c(\epsilon_k)$ an average final-state density function which smooths out the variations with angle and energy caused by diffraction effects. $d\Omega=\sin\theta d\theta d\varphi$ is the element of solid angle.

The total transition rate, $R_t(s)$, is obtained by integrating r_t over all possible initial and final states as well as over the uncertainty, $\delta\epsilon_k$, in the energy of the final state, ϵ_k, introduced by finite lifetimes in initial and final states. This energy uncertainty is introduced by convoluting r_t with a distribution function $I(\delta\epsilon_k,s)$. The I function depends upon s because initial state lifetime depends on r_t which in turn depends on s. $I(\delta\epsilon_k,s)$ specifies the analog of natural linewidth for the Auger neutralization process. Integration over initial states ϵ' and ϵ'' introduces as weighting factors the densities of initial states $N_v(\epsilon')$ and $N_v(\epsilon'')$. The general expression for $R_t(s)$ is then

$$R_t(s)=\int\int\int\int\int\int (2\pi/\hbar)\,|H_{fi}|^2 N_c(\epsilon_k)I(\delta\epsilon_k,s)\times N_v(\epsilon')N_v(\epsilon'')\delta(\epsilon'+\epsilon''+E_i'-\epsilon_0-\epsilon_k-\delta\epsilon_k)d\Omega\times d\epsilon'd\epsilon''d(\delta\epsilon_k)d\epsilon_k. \tag{30}$$

The δ function on energy assures that Eq. (1), with ϵ_k replaced by $\epsilon_k+\delta\epsilon_k$, is satisfied.

$R_t(s)$ is the transition probability per unit time that the Auger neutralization process will occur for ions at a distance s from the solid surface. From it we may obtain another probability distribution, $P_t(s,v_0)$ already defined in Sec. IV such that $P_t(s,v_0)ds$ is the probability that an ion approaching the surface with velocity v_0 will be neutralized in ds at s. In terms of the probability $P_0(s,v_0)$ that an ion reaches s *without* undergoing Auger neutralization we may write

$$P_t(s,v_0)ds=R_t(s)P_0(s,v_0)ds/v_0. \tag{31}$$

P_0 is defined in terms of $R_t(s)$ by

$$P_0(s,v_0)=\exp\left(-\int_s^\infty R_t(s)ds/v_0\right). \tag{32}$$

We now define two other probability distribution functions $P_k(\epsilon_k,s)$ and $P_\Omega(\theta,\epsilon_k,s)$ as follows. $P_k(\epsilon_k,s)ds$ is the probability that the Auger electron produced in a process occurring at s will have energy in the interval $d\epsilon_k$ at ϵ_k. $P_\Omega(\theta,\epsilon_k,s)d\Omega$ is the probability that the Auger electron produced in a process occurring at s and of energy ϵ_k will have a velocity lying in the element of solid angle $d\Omega=\sin\theta d\theta d\varphi$. We assume that P_Ω depends only on θ, the angle with respect to the surface normal inside the solid and not upon the azimuthal angle φ. P_t, P_k, and P_Ω are normalized according to the equations:

$$\int_0^\infty P_t(s,v_0)ds=1, \tag{33}$$

$$\int_{\epsilon_c}^\infty P_k(\epsilon_k,s)d\epsilon_k=1, \tag{34}$$

and

$$\int_0^{2\pi}\int_0^{\pi} P_\Omega(\theta,\epsilon_k,s)\sin\theta d\theta d\varphi=1. \tag{35}$$

In terms of the three probability distributions P_t, P_k, and P_Ω, we may now write the distribution, $N_i(\epsilon_k)$, of

excited electrons inside the solid formed in a sufficiently large number of individual processes. It is

$$N_i(\epsilon_k)=\int_0^\infty\int_0^{2\pi}\int_0^{\pi} P_t(s,v_0)P_k(\epsilon_k,s) \times P_\Omega(\theta,\epsilon_k,s)\,\sin\theta d\theta d\varphi ds. \quad (36)$$

Normalization of P_t by Eq. (33) means that we are assuming all incident ions to undergo Auger neutralization. Equations (33), (34), and (35) result in the normalization of $N_i(\epsilon_k)$ to an area of one electron per incident ion given in Eq. (20).

Electrons in the N_i distribution which approach the surface with sufficient momentum to cross the potential barrier there will escape from the solid. For an electron to be in this class the condition $\theta\leq\theta_c(\epsilon_k)$ must be fulfilled. θ_c is the critical angle for refraction of the electron's velocity into the plane of the surface and depends upon the electron's energy, ϵ_k, and the height of the barrier ϵ_0. For $\theta>\theta_c$ the Auger electron is internally reflected at the surface. The external electron distribution $N_0(\epsilon_k)$ may now be written

$$N_0(\epsilon_k)=\int_0^\infty\int_0^{2\pi}\int_0^{\theta_c} P_t(s,v_0)P_k(\epsilon_k,s) \times P_\Omega(\theta,\epsilon_k,s)\,\sin\theta d\theta d\varphi ds. \quad (37)$$

Equations (36) and (37) may be reduced to more manageable form only if the integrations over θ and s can be separated. Since $R_t(s)$ is a function which increases approximately exponentially with decreasing s, we expect $P_t(s,v_0)$ to be peak shaped and to limit the integration over s to a relatively narrow range. In this range $P_\Omega(\theta,\epsilon_k,s)$ may be approximated by $P_\Omega(\theta,\epsilon_k,s_m)$, where $s=s_m$ is the distance at which the P_t function is maximum (Figs. 3 and 22). When this approximation for P_Ω is made, Eq. (36) reduces to

$$N_i(\epsilon_k)=\int_0^\infty P_t(s,v_0)P_k(\epsilon_k,s)ds, \quad (38)$$

using (35). Equation (37) now reduces to

$$N_0(\epsilon_k)=N_i(\epsilon_k)\int_0^{2\pi}\int_0^{\theta_c} P_\Omega(\theta,\epsilon_k,s_m)\,\sin\theta d\theta d\varphi. \quad (39)$$

The double integral in (39) is the fraction of electrons at ϵ_k in the internal distribution which surmount the surface barrier and is thus the probability of escape already defined in Sec. IV. Its definition in terms of P_Ω is

$$P_e(\epsilon_k)=\int_0^{2\pi}\int_0^{\theta_c} P_\Omega(\theta,\epsilon_k,s_m)\,\sin\theta d\theta d\varphi. \quad (40)$$

Equation (39) is thus a restatement of Eq. (25) introduced earlier.

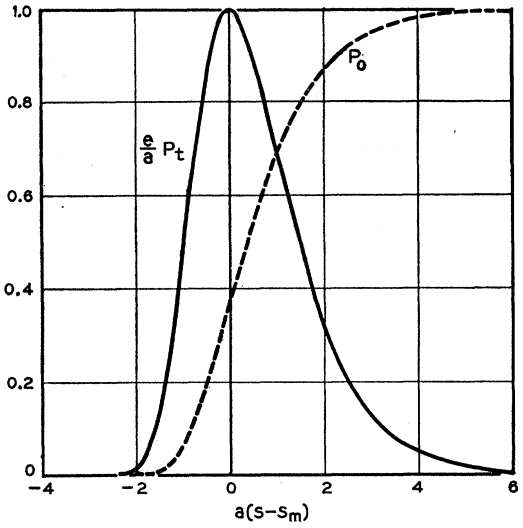

FIG. 22. Plots of the P_0 and P_t functions of Eqs. (42) and (43) in the text. The quantity a in the ordinate is that in Eq. (41) for $R_t(s)$, and s_m is given by Eq. (44).

Of the three probability distributions defined here, we have indicated only how $P_t(s,v_0)$ in Eqs. (31) and (32) is related to the transition rate $R_t(s)$ and hence to the matrix element through Eq. (30). Both the $P_k(\epsilon_k,s)$ and $P_\Omega(\theta,\epsilon_k,s_m)$ distributions must also relate in a fundamental way to the energy and angle dependences of the matrix element as will be seen.

It is instructive to look at the properties of the P_t function for an exponential rate function of the form

$$R_t(s)=A\,\exp(-as). \quad (41)$$

Equation (32) gives

$$P_0(s,v_0)=\exp[-(A/av_0)\,\exp(-as)], \quad (42)$$

and Eq. (31),

$$P_t(s,v_0)=(A/v_0)\,\exp[-(A/av_0)\,\exp(-as)-as]. \quad (43)$$

This P_t function passes through a maximum at $s=s_m$ with

$$s_m=(1/a)\,\ln(A/av_0), \quad (44)$$

and its value there is

$$P_t(s_m)=a/e=0.368a, \quad (45)$$

independent of v_0. A graphical solution for the width of the P_t function of Eq. (43) at half maximum gives

$$W(P_t)=2.48/a. \quad (46)$$

Written in terms of s_m, expressions (42) and (43) become

$$P_0(s,v_0)=\exp\{-\exp[-a(s-s_m)]\}, \quad (47)$$

and

$$P_t(s,v_0)=a\,\exp\{-\exp[-a(s-s_m)]-a(s-s_m)\}. \quad (48)$$

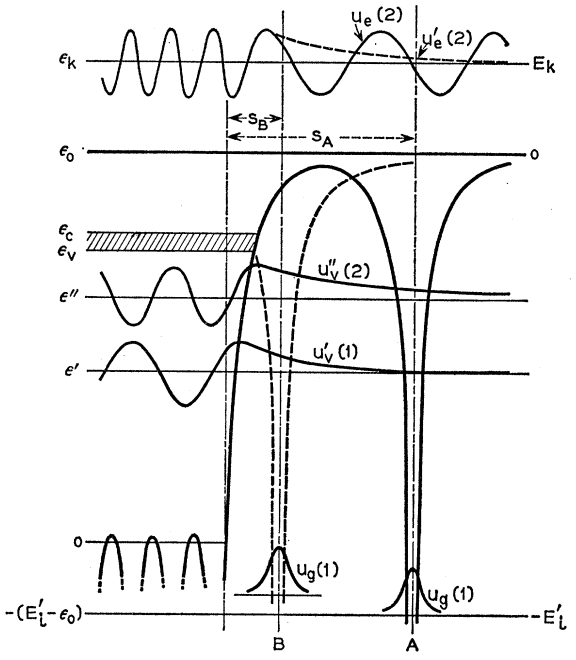

FIG. 23. Schematic representation of electronic wave functions plotted on an electron energy diagram like that of Fig. 2. Two positions of the atom outside the solid are shown at A and B. Two wave functions for the excited electron at ϵ_k are shown. One, u_e, corresponds to electrons which cross the potential barrier at the surface ($\theta<\theta_c$). The other, u_e', represents electrons internally reflected at the surface barrier ($\theta>\theta_c$).

These two functions are plotted in Fig. 22. Equations (45), (46), and (48) indicate that for an exponential rate function the form of P_t is independent of v_0. The position of P_t relative to the solid surface, however, is determined by v_0 through s_m [Eq. (44)]. It can be shown[12] that the mean distance of Auger neutralization under these circumstances is close to s_m.

XII. THE MATRIX ELEMENT

We turn now to a discussion of the matrix element. We shall first introduce the wave functions and discuss the effects of their antisymmetrization. The initial state wave functions are u_v' and u_v'' for electrons at ϵ' and ϵ'' in the valence band, respectively. The final state functions are u_g and u_e for electrons in the ground atomic state and in an excited state at ϵ_k in the conduction band, respectively. Figure 23 shows schematic representations of these four functions. We note that each of the two u_e functions has an appropriate range of θ. The functions u_v' and u_v'' are periodic inside the lattice but fall off exponentially at sufficiently great distances outside the surface. u_g is the spherically symmetric s function of the ground state of the noble gas atom. u_e can take either of two forms, depending upon whether the electron is transmitted through or internally reflected at the surface barrier. u_e in Fig. 23 corresponds to transmission ($\theta<\theta_c$) and is periodic but of different wavelength on the two sides of the barrier. u_e' corresponds to the case of internal reflection ($\theta>\theta_c$) and, like the valence band functions, has an exponential tail outside the solid.

Consider now angular dependence and normalization of the electron wave functions. For a plane barrier the tails of the u_v functions outside the solid will vary as $\exp\{-[2m(\epsilon_0-\epsilon\cos^2\theta)]^{\frac{1}{2}}s/\hbar\}$, which decreases in magnitude at any s if either θ is increased at constant ϵ, or ϵ decreased at constant θ. In the discussion which follows, it is necessary only that the two u_v functions be normalized in the same manner. The u_e and u_e' functions are normalized on a flux basis, each representing the flux of one Auger electron as it passes over or is reflected by the surface barrier. For given ϵ_k the wavelengths of u_e and u_e' inside the solid are the same although the range of θ is different for the two functions. Again, for a plane barrier, the magnitude of u_e' outside the solid varies as the exponential given above with $\theta>\theta_c$ $=\cos^{-1}(\epsilon_0/\epsilon_k)^{\frac{1}{2}}$ [Eq. (102)].

Neglecting spin we may write two "elemental" matrix elements corresponding to the two sets of transitions shown in Fig. 2. The matrix element

$$H'=\int\int u_g^*(1)u_e^*(2)(e^2/r_{12})u_v'(1)u_v''(2)d\tau_1 d\tau_2 \quad (49)$$

corresponds to transitions 1, 2 of Fig. 2 and

$$H''=\int\int u_g^*(2)u_e^*(1)(e^2/r_{12})u_v'(1)u_v''(2)d\tau_1 d\tau_2 \quad (50)$$

corresponds to transitions 1′, 2′. In these expressions the numbers in parentheses indicate the space coordinates of electrons 1 and 2. The perturbation is the Coulomb interaction, e^2/r_{12}, between the participating electrons. For a metal one expects this interaction to be screened and for a semiconductor to be reduced by the dielectric constant. Such effects will be dependent on distance from the surface and will thus contribute to the form of the rate function, $R_t(s)$. Since the exact nature of the interaction does not affect the basic conclusions reached here, it will not be considered further.

We must now introduce spin and take account of the Pauli principle by antisymmetrizing the wave functions. Symmetric and antisymmetric orthonormal space functions for the final states may be written as:

$$u_f^{\pm}=2^{-\frac{1}{2}}[u_g^*(1)u_e^*(2)\pm u_g^*(2)u_e^*(1)]. \quad (51)$$

The functions,

$$u_i^{\pm}=2^{-\frac{1}{2}}[u_v'(1)u_v''(2)\pm u_v'(2)u_v''(1)], \quad (52)$$

are similar space functions for the initial states. As spin wave functions we use the usual orthonormal functions,

[12] Equations (45)–(47) and accompanying text in reference 5.

three of which are symmetric:

$$s_1=\alpha(1)\alpha(2), \tag{53}$$

$$s_2=2^{-\frac{1}{2}}[\alpha(1)\beta(2)+\beta(1)\alpha(2)], \tag{54}$$

$$s_3=\beta(1)\beta(2), \tag{55}$$

and one antisymmetric:

$$s_4=2^{-\frac{1}{2}}[\alpha(1)\beta(2)-\beta(1)\alpha(2)]. \tag{56}$$

The four final-state and four initial-state antisymmetric wave functions which result from all possible combinations of the above space and spin functions are $u_f^-s_1$, $u_f^-s_2$, $u_f^-s_3$, $u_f^+s_4$, $u_i^-s_1$, $u_i^-s_2$, $u_i^-s_3$, $u_i^+s_4$. By virtue of spin function orthogonality only four matrix elements remain of the 16 possible using these 8 functions. Using the normalization properties of the spin functions, these four matrix elements may be written out and reduced to expressions in terms of the "elemental" matrix elements H' and H'' of expressions (49) and (50). The results are *three* integrals of the form,

$$H_a=\int u_f^-(e^2/r_{12})u_i^-d\tau_1d\tau_2=H'-H'', \tag{57}$$

derived from the three sets of functions involving the antisymmetric space function, and *one* integral of the form

$$H_b=\int u_f^+(e^2/r_{12})u_i^+d\tau_1d\tau_2=H'+H'', \tag{58}$$

derived from the single set of functions involving the symmetric space function. These represent the four distinguishable elemental Auger processes involving electrons initially at specific energies ϵ' and ϵ'' in the valence band when spin is accounted for. The term $|H_{fi}|^2$ in expression (30) is to be replaced by the sum of the squares of the four matrix elements. When this is done, we obtain

$$|H_{fi}|^2=\tfrac{1}{4}[3H_a^2+H_b^2]=[H'^2+H''^2-H'H''], \tag{59}$$

in which we have divided out the numerical factor 4 resulting from the total number of ways the spins of the two electrons can be arranged.

Expression (59) is to be compared with the corresponding expression obtained, if the Pauli principle is neglected:

$$|H_{fi}|^2=[H'^2+H''^2]. \tag{60}$$

We see that if $H'=H''$, the Pauli principle results in a decrease of a factor 2 in the transition rate. This factor merely changes slightly the distance at which the process occurs and is unimportant. What is important is the possible energy dependence of $|H_{fi}|^2$ introduced by the functional dependence of expression (59). Our expression for the total matrix element can be shown to be consistent with that given by Burhop.[13] For the three symmetric spin functions Burhop's $f_1^n=H'$ and $f_2^n=H''$, thus making his $f_1^n-f_2^n=H'-H''=H_a$. For the single antisymmetric spin function Burhop's $f_1^n=H'$ and $f_2^n=-H''$ yielding $f_1^n-f_2^n=H'+H''=H_b$. When the four corresponding b_n' given by his Eq. (2.12) are added one obtains the sum of squares given here in expression (59).

We may express the total matrix element taking account of the Pauli principle in more convenient form as follows. Let us assume that $H'\geq H''$ and write

$$H''=mH', \quad 0\leq m\leq 1. \tag{61}$$

Then expression (59) becomes

$$|H_{fi}|^2=H'^2[1-m+m^2]=H'^2[\tfrac{3}{4}+(m-\tfrac{1}{2})^2]. \tag{62}$$

Thus H_{fi} as a function of m is symmetrical about its lowest value at $m=\frac{1}{2}$ at which point $|H_{fi}|^2=\frac{3}{4}H'^2$.

We shall now introduce a way of looking at the matrix element, H' say, which brings to light its possible dependencies on energy and angle. Rewriting expression (49) in such a way as to group together functions in the coordinates of a single electron on each side of the perturbation term, we obtain

$$H'=\int\int u_g^*(1)u_v'(1)(e^2/r_{12})u_e^*(2)u_v''(2)d\tau_1d\tau_2. \tag{63}$$

We now see that H' has the form of a Coulomb interaction energy between two charge clouds $eu_g^*(1)u_v'(1)=eF(1)$ and $eu_e^*(2)u_v''(2)=eG(2)$. Because the atomic ground state, for He at least, lies farther below the vacuum level than do the valence states, $F(1)$ will be a function limited to the vicinity of the atom. Its magnitude will vary with ϵ through the valence band as does the u_v' function at the atom position. The matrix element is then the integral of the product of $F(1)$ and $G(2)$ weighted by the inverse distance between electrons, $1/r_{12}$. Here $u_e^*(2)$ is the complex conjugate of either u_e or u_e' shown in Fig. 23 as appropriate.

The picture of the matrix element as a Coulomb interaction integral leads to the following possible energy dependences:

(1) A dependence on $\epsilon_0-\epsilon'$ and $\epsilon_0-\epsilon''$, the depths of the valence energy levels below the vacuum level, by virtue of the $\exp\{-[2m(\epsilon_0-\epsilon\cos^2\theta)]^{\frac{1}{2}}s/\hbar\}$ term in the u_v functions.

(2) A direct dependence on ϵ' and ϵ'' brought about by the change in symmetry character of the u_v functions with energy.

(3) An energy dependence on $(\epsilon''-\epsilon')$ arising from exchange matrix element cancellation as expressed in Eqs. (59) or (62).

[13] E. H. S. Burhop, *The Auger Effect and Other Radiationless Transitions* (Cambridge University Press, New York, 1952), p. 15, Eq. (2.12).

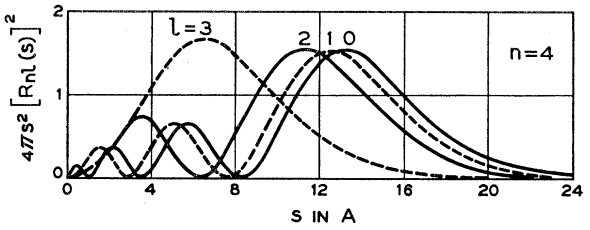

FIG. 24. Plots of the radial distributions of electrons in the $n=4, l=0$, 1, 2, and 3 orbitals of the hydrogen atom. Here the radius is designated by s.

We shall discuss each of these items in turn. Each dependence will, in general, depend on s, which fact must also be discussed.

For neutralization at large s (position A in Fig. 23), the dependence on $\epsilon_0-\epsilon'$ and $\epsilon_0-\epsilon''$ should be marked. It is a very strong dependence and would limit participation in the Auger process to only those electrons which lie at the top of the valence band. That this is not the case can be seen directly in the experimental data of Fig. 1. Here for He^+ we observe Auger electrons over a range of energy 12 ev wide. This means that we are observing electrons which come from the valence band to an average depth in the band 6 ev below the top. For neutralization close to the surface (position B in Fig. 23) where the barrier between solid and atom is thin and the exponential tails of the u_v functions are not well developed, we should expect the dependence on $\epsilon_0-\epsilon'$ and $\epsilon_0-\epsilon''$ to be small or nonexistent. From the fact that the theoretical fit to the experimental data given in Sec. VI requires that transition rate *decrease* as ϵ increases, we conclude that the ion is neutralized sufficiently close to the surface to prevent any appreciable dependence on depth in the well (item 1 above).

The direct dependence on ϵ' and ϵ'' brought about by change in symmetry character of the u_v functions from s to p as ϵ increases (item 2) rests upon the fact that at a given distance a p-wave function is smaller in magnitude than an s function of the same energy. This can be seen from a plot of radial distributions of hydrogenic wave functions of the same energy. In Fig. 24 such distributions are plotted for the s, p, d, and f electrons having $n=4$. For distances from the nucleus[14] greater than 14 A we are in the tails of these functions and the s function is greater than the p, the p than the d, etc. The large distances in this example come from the choice of the $n=4$ shell for illustrative purposes and are not indicative of distances to be expected in the Auger neutralization process.

We may estimate the magnitude of the ratio of transition probabilities for s and p electrons in the following way using Hartree wave functions for germanium. We take the radial part of the atomic wave function to be of the form,[14]

$$P(s)=f(s)\exp[-(2mE_i/\hbar^2)^{\frac{1}{2}}s]. \quad (64)$$

Here $f(s)$ includes the dependence on angular momentum. The exponential term gives for the atom the energy dependence on depth in the potential well analogous to the $(\epsilon_0-\epsilon)$ dependence discussed above. Hartree, Hartree, and Manning[15] give values of $P(s)$ for the $4s$ and $4p$ electrons of Ge. The energies required to ionize these electrons are 63 600 cm^{-1} [GeI($4s^24p^2\,^3P_0$) to GeII($4s^24p\,^2P_{0,\frac{1}{2}}^0$)] for the $4p$ electron, and 115 600 cm^{-1} [GeI($4s^24p^2\,^3P_0$) to GeII($4s4p^2\,^4P_{0,\frac{1}{2}}$)] for the $4s$ electron.[16] One can then calculate the ratio r of the squares of the $f(s)$ functions by correcting for the exponential dependence on E_i according to the expression:

$$r=\left[\frac{f_{4p}(s)}{f_{4s}(s)}\right]^2=\frac{P_{4p}(s)}{P_{4s}(s)}\times\exp\{-(2m/\hbar^2)^{\frac{1}{2}}[E_i^{\frac{1}{2}}(4p)-E_i^{\frac{1}{2}}(4s)]s\}. \quad (65)$$

This quantity is plotted in Fig. 25 where s is now taken as the distance from the solid germanium surface.

As discussed in Sec. IV, a direct dependence on ϵ' and ϵ'' can be accounted for in the theory by the use of the effective state density $N_v'(\epsilon)=q(\epsilon)N_v(\epsilon)$ defined in Eq. (13). By Eq. (30) the transition rate R_t will then depend on q^2. Since $|H_{fi}|$ depends on the product of two u_v functions, we expect it to depend directly on r of Eq. (65) and R_t by (30) on r^2. Thus, $q(\epsilon)$ should depend on the first power of r as indeed was assumed in Eqs. (14) and (15). If we take $s=2.2$ A, the nearest neighbor distance in germanium, as a reasonable distance at which Auger neutralization occurs we find that Fig. 25 predicts $r\sim0.3$, the value found in the fit to experiment in Sec. VI. This numerical agreement indicates a basic consistency between the distance at which the process occurs and the nature of the energy dependence which is operative.

The third possible energy dependence listed above is that involving exchange matrix element cancellation arising in the $(1-m+m^2)$ term of Eq. (62). We expect m to be a function of the energy difference $(\epsilon''-\epsilon')$ between the initial electronic states. For $\epsilon''=\epsilon'$, $m=1$ and $|H_{fi}|^2=H'^2$. For $\epsilon''\neq\epsilon'$, m may vary from unity but the dependence of H_{fi} on m is such that it can never fall below $\frac{3}{4}H'^2$, its value for $m=\frac{1}{2}$. Electron exchange changes $F(1)$ from $u_g^*(1)u_v'(1)$ to $u_g^*(1)u_v''(1)$ and $G(2)$ from $u_e^*(2)u_v''(2)$ to $u_e^*(2)u_v'(2)$. This interchange would have no effect if the range of integration limited the significant parts of the $G(2)$ function to a volume about the atom as small as that in which the $F(1)$ function has value. Even though the volume over

[14] Since r has been used as a parameter, we shall use s in this discussion for distance from a free atomic nucleus as well as distance from the solid surface defined as distance from the outermost nuclei in the solid.

[15] W. Hartree, D. R. Hartree, and M. F. Manning, Phys. Rev. **59**, 306 (1941).

[16] Atomic energy level data are taken from C. E. Moore, *Atomic Energy Levels*, National Bureau of Standards Circular No. 467 (U. S. Government Printing Office, Washington, D. C., 1952), Vol. II.

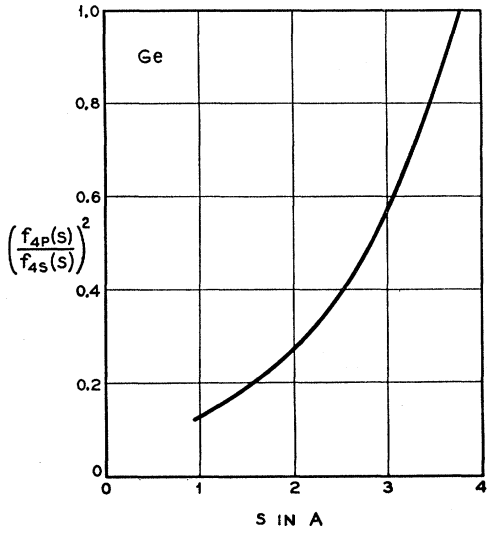

FIG. 25. Plot of the quantity $(f_{4p}/f_{4s})^2$, calculated from the Hartree wave functions for germanium as discussed in the text of Sec. XII.

which $G(2)$ is integrated is significantly greater than the volume in which $F(1)$ has value, changes in F and G brought about by interchange of the u_v functions will certainly tend to compensate. We thus expect the parameter m not to depart too drastically from unity and that $|H_{fi}|^2 \sim H'^2$.

Any energy dependence introduced by the $(1-m+m^2)$ term should of the following kind. $(1-m+m^2)$ can depart farthest from unity when the integration in expression (30) over ϵ' and ϵ'' extends over the greatest range, that is when ϵ, the mean of ϵ' and ϵ'', lies near the center of a band or subband. As ϵ' and ϵ'' both approach the same edge of a band their difference decreases and $|H_{fi}|^2$ approaches H'^2. Thus, any energy dependence introduced by the $(1-m+m^2)$ term should be representable by a function which is symmetric about the center of a band and approaches unity at the edges. This symmetry is the same as that of the functions used to specify the state density function, $N_v(\epsilon)$. Hence, an energy dependence introduced by exchange matrix element cancellation, if it exists at all, could not be separated from the form of the $N_v(\epsilon)$ function. It perhaps should be included among the minor variations with energy discussed under $P_e(\epsilon_k)$ in Sec. VIII and in Sec. XV.

Finally, H_{fi} could also depend on the angles θ and φ. The picture of the matrix element as a Coulomb interaction integral indicates that a dependence on θ will arise by virtue of the difference in magnitudes of the u_e and u_e' functions outside the solid and the fact that they apply over different ranges of θ. The u_e function representing escaping electrons for which $\theta<\theta_c$ is larger in magnitude in the vicinity of the atom than is the u_e' function which applies for $\theta>\theta_c$. Further, the tail of the u_e' function decreases in magnitude as θ increases above θ_c. Thus the matrix element might be expected to change rather abruptly at $\theta=\theta_c$ where the final state wave function changes from $u_e(\theta<\theta_c)$ to $u_e'(\theta>\theta_c)$ and to decrease with further increase in θ above θ_c.

One might expect H_{fi} to depend upon φ as a result of surface atomicity of the solid and possible dependence on impact parameter relative to a given surface atom. It appears not unreasonable to suppose, however, that such differences average out to independence of φ on integration over the surface.

The above discussion indicates that we expect the principal energy dependence of the matrix element to be a direct dependence on ϵ' and ϵ'' which can be accounted for by an effective state density function for the initial states. This validates the assumptions leading to Eqs. (13), (14), and (15) and illuminates the first conclusion of Sec. X. Dependence of H_{fi} on θ may be accounted for in terms of the angular probability distribution $P_\Omega(\theta,\epsilon_k,s_m)$ of Sec. XI. These conclusions concerning the matrix element are incorporated in the theory by writing

$$|H_{fi}|^2=(\hbar/2\pi)Cq(\epsilon')q(\epsilon'')P_\Omega(\theta,\epsilon_k,s_m), \qquad (66)$$

in which C is a constant. Integrations over energy and angle are now separable in Eq. (30) which, using Eq. (13), reduces to

$$R_t(s)=C\int\int\int\int\int\int N_c(\epsilon_k)I(\delta\epsilon_k,s)N_v'(\epsilon')N_v'(\epsilon'')\times\delta(\epsilon'+\epsilon''+E_i'-\epsilon_0-\epsilon_k-\delta\epsilon_k)P_\Omega(\theta,\epsilon_k,s_m)\times d\Omega d\epsilon' d\epsilon'' d(\delta\epsilon_k)d\epsilon_k. \qquad (67)$$

XIII. THE AUGER TRANSFORM AND THE INTRODUCTION OF ENERGY BROADENING

We now consider the double integral,

$$\int\int N_v'(\epsilon')N_v'(\epsilon'')\times\delta(\epsilon'+\epsilon''+E_i'-\epsilon_0-\epsilon_k-\delta\epsilon_k)d\epsilon' d\epsilon'', \qquad (68)$$

to be found in expression (67). Changing variables from ϵ' and ϵ'' to ϵ and Δ, we obtain

$$\int\int N_v'(\epsilon-\Delta)N_v'(\epsilon+\Delta)\delta(2\epsilon+E_i'-\epsilon_0-\epsilon_k-\delta\epsilon_k)d\Delta d\epsilon = \int T(\epsilon)\delta(2\epsilon+E_i'-\epsilon_0-\epsilon_k-\delta\epsilon_k)d\epsilon = T[\tfrac{1}{2}(\epsilon_k+\delta\epsilon_k+\epsilon_0-E_i')], \qquad (69)$$

in which $T(\epsilon)$ is the Auger transform of Eq. (16). Making use of (68) and (69), expression (67) reduces to

$$R_t(s)=C\int\int\int N_c(\epsilon_k)I(\delta\epsilon_k,s)\times T[\tfrac{1}{2}(\epsilon_k+\delta\epsilon_k+\epsilon_0-E_i')]P_\Omega(\theta,\epsilon_k,s_m)\times d\Omega d(\delta\epsilon_k)d\epsilon_k. \qquad (70)$$

Integrating over angle and inserting integration limits, we obtain

$$R_t(s)=C\int_{\epsilon_c}^{\infty}\int_{-\infty}^{\infty}N_c(\epsilon_k)I(\delta\epsilon_k,s)\times T[\tfrac{1}{2}(\epsilon_k+\delta\epsilon_k+\epsilon_0-E_i')]d(\delta\epsilon_k)d\epsilon_k. \quad (71)$$

We now make use of the identity,

$$R_t(s)\equiv\int_{\epsilon_c}^{\infty}R_t(s)P_k(\epsilon_k,s)d\epsilon_k, \quad (72)$$

which results from the normalization condition (34) on the P_k function. Comparison of Eqs. (71) and (72) leads to the following expression for the $P_k(\epsilon_k,s)$ probability distribution:

$$P_k(\epsilon_k,s)=\frac{N_c(\epsilon_k)\int_{-\infty}^{\infty}I(\delta\epsilon_k,s)T[\tfrac{1}{2}(\epsilon_k+\delta\epsilon_k+\epsilon_0-E_i')]d(\delta\epsilon_k)}{\int_{\epsilon_c}^{\infty}\int_{-\infty}^{\infty}N_c(\epsilon_k)I(\delta\epsilon_k,s)T[\tfrac{1}{2}(\epsilon_k+\delta\epsilon_k+\epsilon_0-E_i')]d(\delta\epsilon_k)d\epsilon_k}. \quad (73)$$

At this point one could perform the integration over $\delta\epsilon_k$ indicated in the above expressions using a suitable distribution $I(\delta\epsilon_k,s)$. This would account for the energy broadening due to finite lifetimes of initial and final states. However, it is expedient to delay this step until somewhat later in the development when it can be coupled with a similar integration to account for energy broadening caused by the finite width of the $P_t(s,v_0)$ distribution and the variation of atomic energy levels with distance from the solid surface.

Equation (73) relates $P_k(\epsilon_k,s)$ to the matrix element of the Auger process and its integration over initial states. Putting it into Eq. (38) and neglecting the normalization factor, we obtain

$$N_i(\epsilon_k)\propto N_c(\epsilon_k)\int_0^{\infty}\int_{-\infty}^{\infty}P_t(s,v_0)I(\delta\epsilon_k,s)\times T[\tfrac{1}{2}(\epsilon_k+\delta\epsilon_k+\epsilon_0-E_i')]d(\delta\epsilon_k)ds. \quad (74)$$

We note that T is a function of s through E_i' which depends on s.

The integrations over s and $\delta\epsilon_k$ in (74) can be shown to be successive convolutions of the T function by the I and P_t functions and thus to represent a broadening of the T function. Again using the fact that the expected form of the P_t function limits the integrand of (74) to a relatively narrow range of s, we may replace $I(\delta\epsilon_k,s)$ by $I(\delta\epsilon_k,s_m)$ and $E_i'(s)$ by

$$E_i'(s)\cong E_i'(s_m)+k(s-s_m), \quad (75)$$

in which

$$k=[dE_i'/ds]_{s=s_m}. \quad (76)$$

Since $P_t(s,v_0)$ is zero for $s<0$, we may replace the lower integration limit of zero for s in (74) with $-\infty$. The nature of the double integral in expression (74), which we call the broadened Auger transform $T_b(\epsilon)$, is seen more clearly if we write it in terms of ϵ, where

$$2\epsilon=\epsilon_k+\delta\epsilon_k+\epsilon_0-E_i'(s_m). \quad (77)$$

and let

$$y=-k(s-s_m)/2, \quad (78)$$

$$z=\delta\epsilon_k/2. \quad (79)$$

P_t and I are then functions of y and z, respectively, and the double integral in (74) becomes

$$T_b(\epsilon)=\int_{-\infty}^{\infty}\int_{-\infty}^{\infty}P_t(s_m-2y/k)I(2z)T(\epsilon+y+z)dydz. \quad (80)$$

In the calculations outlined in Sec. V broadening of the $T(\epsilon)$ function was accomplished by a single convolution with a Gaussian function [Eq. (17)]. Equation (80) will reduce to (17) if $P_t(s_m-2y/k)$ and $I(2z)$ are replaced by Gaussian functions which we shall designate $\varphi_{\sigma_1}(y)$ and $\varphi_{\sigma_2}(z)$, respectively. These successive convolutions with the Gaussian function are the equivalent of a single convolution with a Gaussian function for which

$$\sigma=(\sigma_1^2+\sigma_2^2)^{\frac{1}{2}}. \quad (81)$$

Formula (17) appears to be a good approximation to (80) for low ion energies where broadening is small but introduces significant error in detail at higher ion energies where broadening is important.

Equation (74) leads to the following expression for $N_i(\epsilon_k)$ in terms of $T_b(\epsilon)$:

$$N_i(\epsilon_k)=\frac{N_c(\epsilon_k)T_b[\tfrac{1}{2}(\epsilon_k+\epsilon_0-E_i'(s_m))]}{\int_{\epsilon_c}^{\infty}N_c(\epsilon_k)T_b[\tfrac{1}{2}(\epsilon_k+\epsilon_0-E_i'(s_m))]d\epsilon_k}. \quad (82)$$

Equation (82) reduces to Eq. (19) if $N_c(\epsilon_k)$ is taken to be constant or its energy dependence subsumed into the $P_e(\epsilon_k)$ function (Sec. XV).

Convolution of $T(\epsilon)$ with the P_t function in Eq. (80) accounts for the variation in energy of the atomic ground state over the range of distances, specified by the P_t function, in which the Auger transitions occur. The form of the P_t function for exponential $R_t(s)$ plotted in Fig. 22 is not unlike the Gaussian function.

Broadening by the P_t function is in fact more symmetrical than the plot of P_t on the s scale indicates by virtue of the fact that $E_i'(s)$, contrary to the simple assumption of Eqs. (75) and (76), varies more rapidly for $s<s_m$ than for $s>s_m$. If the P_t function in Eq. (80) is replaced by a Gaussian function $\varphi_{\sigma 1}(y)$ of equal width at half maximum and if an exponential rate function is assumed, we may calculate σ_1 as follows. The width of the P_t function at half maximum on the s scale is then $(2.48/a)$ by Eq. (46). From (78) this width on the y scale is $1.24k/a$. Using (76) we obtain

$$W(\varphi_{\sigma 1})=(1.24/a)[dE_i/ds]_{s=s_m}. \tag{83}$$

The relation between the parameter σ in the Gaussian function [Eq. (18)] and the width at half maximum, $W(\varphi_\sigma)$, is

$$\sigma=W(\varphi_\sigma)/2.36. \tag{84}$$

From (83) and (84) we obtain

$$\sigma_1=(0.53/a)[dE_i'/ds]_{s=s_m}. \tag{85}$$

We may estimate values for σ_1 only after we know more about the functional dependence of the effective ionization energy, $E_i'(s)$.

Convolution by the I function in Eq. (80) accounts for energy broadening by virtue of finite lifetimes in initial and final states and the Heisenberg principle. Broadening due to initial-state lifetime here should resemble natural line broadening which is characterized by the Lorentzian function. Neglecting, for the moment, finite lifetime in the final state, $I(\delta\epsilon_k,s_m)$ should be given by

$$I(\delta\epsilon_k,s_m)=1/\{(\delta\epsilon_k)^2+[\tfrac{1}{2}\hbar R_t(s_m)]^2\}. \tag{86}$$

Approximating this by a Gaussian is poorer the greater $R_t(s_m)$. However, if this approximation is made and widths at half maximum are again equated, one calculates

$$W(\varphi_{\sigma 2})=\tfrac{1}{2}\hbar R_t(s_m)=\tfrac{1}{2}\hbar a v_0. \tag{87}$$

This results from the fact that the width of $I(\delta\epsilon_k,s_m)$ at half maximum is $\hbar R_t(s_m)$ on the $\delta\epsilon_k$ scale and from the use of Eqs. (79), (41), and (44). From (84) we obtain[17]

$$\sigma_2=0.212\hbar a v_0. \tag{88}$$

We reiterate that the values of σ_1 and σ_2 just derived are based on the approximation of the P_t and I functions by Gaussian functions and the assumption of an exponential rate function, $R_t(s)$.

Final-state lifetime arises because the holes left by the Auger neutralization process at ϵ' and ϵ'' in the valence band are filled by secondary Auger processes involving electrons lying higher in the band. These processes are of the type proposed by Skinner[18] to account for tailing observed at the long-wavelength limit in the soft x-ray spectra of metals. Landsberg[19] has shown that this broadening for metals is maximum for holes at the bottom of the band and falls to zero as the holes are moved to the top. In semiconductors this broadening should fall to zero at a point lying below the top of the band by a forbidden gap width, since holes can rise no higher than this in subsidiary Auger processes involving transition of electrons across the gap. Thus the final-state broadening is least significant for the upper part of the valence band which is of most interest in this work.

We further observe that, unlike initial-state broadening, final-state broadening is independent of ion velocity. Thus final-state broadening can be no larger than that needed to account for all broadening for the slowest ions. Estimates to be made presently of initial-state broadening and broadening due to variation of the energy of the atomic ground state with distance indicate that together they can account for the broadening observed for 10-ev ions, leaving little to be ascribed to final-state broadening. This conclusion is corroborated by an estimate of final-state lifetime based on a mean free path for pair production estimated by Wolff.[20] Wolff[21] considers his value of 15 A for this mean free path to be essentially what one would expect for a hole at midband in the present case. Taking the hole velocity to be 10^{16} A sec^{-1}, one obtains a lifetime of 1.5×10^{-15} sec. This leads by the Heisenberg principle to an energy uncertainty of 0.4 ev. Taking this to be another $\delta\epsilon_k$ like that in Eq. (79), it leads to a width $W(\varphi_{\sigma 3})$ at half maximum of a third convoluting Gaussian $\varphi_{\sigma 3}$ equal to $0.4/2=0.2$ ev on the z scale. σ_3 from Eq. (84) would then be $0.2/2.36=0.08$. It contributes little to broadening for 10-ev ions for which $\sigma=0.3$ because the components of σ combine as the square root of the sum of squares [Eq. (81)]. Bronshtein and Segal'[22] give values for the range of slow secondary electrons in several metals which vary from 7 to 12 atomic layers. These results imply a somewhat longer free path, greater lifetime, and hence smaller broadening than does Wolff's estimate. One appears to be on safe ground in neglecting entirely broadening effects due to final state lifetime.

XIV. EFFECTIVE IONIZATION ENERGY AND THE MAGNITUDE OF ENERGY BROADENING

We turn now to a discussion of the effective ionization energy near the solid surface. We have seen that it enters into the theory directly in the change of variable

[17] This equation differs from that given in Eq. (87) in reference 5 by a factor 2. The equation in reference 5 is in error because of the neglect there of the relation between $\delta\epsilon_k$ and z [Eq. (79) in the present work]. Note also that there is a confusion of y and z in Eqs. (78) and (79) of reference 5.

[18] H. W. B. Skinner, Phil. Trans. Roy. Soc. London **A239**, 95 (1940).

[19] P. T. Landsberg, Proc. Phys. Soc. (London) **A62**, 806 (1949).

[20] P. A. Wolff, Phys. Rev. **95**, 1415 (1954), Sec. II.

[21] P. A. Wolff (private communication).

[22] I. M. Bronshtein and R. B. Segal', Fizika Tverdogo Tela **1**, 1489 and 1500 (1959) [translation: Soviet Phys.-Solid State **1**, 1365 and 1375 (1956)].

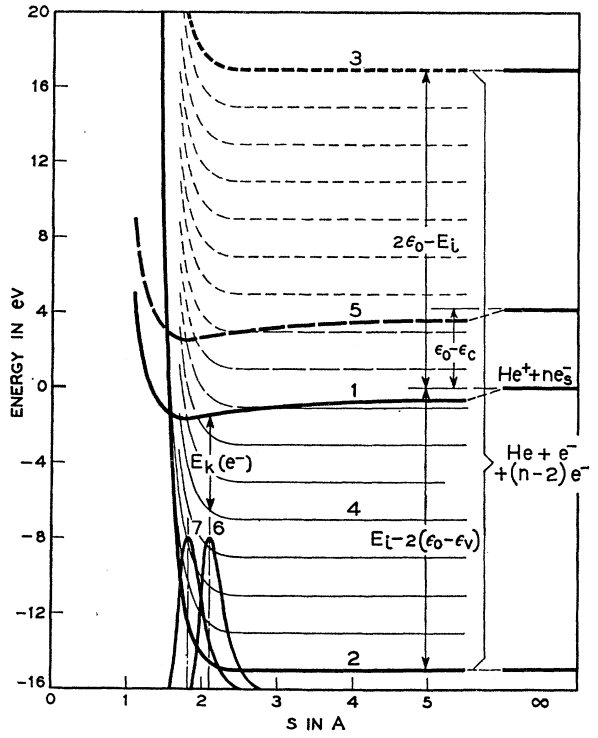

FIG. 26. Potential energy diagram for the Auger neutralization process [Eq. (89)] discussed in the text of Sec. XIV.

from ϵ to ϵ_k [Eqs. (19) and (82)] and that the fit of theory to experiment yields an empirical dependence of E_i-E_i' on ion energy [Eq. (27)]. $[dE_i'/ds]_{s=s_m}$ helps to determine energy broadening through Eq. (85). In this section we shall investigate the dependence of E_i' on distance s between atom and solid and shall show that the second and third conclusions of the theoretical fit to experiment listed in Sec. X are reasonable in terms of more basic theory.

The dependence of E_i' on s is best discussed in terms of a potential energy diagram for the whole system of atom and solid. Such a diagram for the Auger neutralization of He^+ at the (111) face of silicon or germanium is shown in Fig. 26. This diagram is to be distinguished from that of Fig. 2 which is an electron energy level diagram. In Fig. 26 we consider the Auger process as the transformation of the system consisting initially of the He^+ ion and n electrons, e_S^-, in the semiconductor to the isoelectronic system of the neutralized He atom, a free electron e^-, and $(n-2)$ electrons remaining in the solid. The Auger process may thus be written

$$He^+ + ne_S^- \rightarrow He + e^- + (n-2)e_S^-. \quad (89)$$

The initial state in Eq. (89), $He^+ + ne_S^-$ for He^+ at rest at $s=\infty$, has a discrete energy which we take to be zero. The final state, $He + e^- + (n-2)e_S^-$ for He and e^- at rest at $s=\infty$, may have potential energy anywhere in a band extending from $2\epsilon_0-E$ to $-[E_i-2(\epsilon_0-\epsilon_v)]$. These limits may be derived from the energy transformations dictated by Eq. (89) at $s=\infty$ neglecting the forbidden gap and the Pauli principle and assuming that one can choose the two electrons to lie initially at any energy in the valence band.

As s is decreased toward zero, both initial and final states will vary in energy. The initial state will vary with s as does the interaction energy, $E(i,S)$, between the ion (i) and the solid (S). $E(i,S)$ should involve the image potential and a repulsive term. The Van der Waals interaction is completely negligible compared to the energy discrimination of the experiment and is neglected. We also neglect the possibility of covalent bonding between ion and solid. Thus we write

$$E(i,S) = -(\kappa-1)e^2/4(\kappa+1)s + B_i \exp(-b_i s), \quad (90)$$

in which κ is the dielectric constant of the semiconductor. The final state varies with s as does the interaction $E(n,S)$ between the neutral atom (n) and the solid (S), for which we write

$$E(n,S) = B_n \exp(-b_n s), \quad (91)$$

again neglecting any Van der Waals interaction. Curves 1 and 5 in Fig. 26 are plots of Eq. (90), curves 2 and 3 of Eq. (91). Each curve is plotted with respect to its corresponding asymptote at $s=\infty$.

Also plotted in Fig. 26 are two $P_t(s,v_0)$ distributions, curves 6 and 7 for 10-ev and 1000-ev ions, respectively. These are plots of Eqs. (43) or (48) for the case of an exponential rate function. Note that as incident velocity increases P_t moves closer to the surface as Eq. (44) demands. Values of the parameters used in the curves of Fig. 26 were obtained as the preliminary results of a program mentioned later in this section. For our present purposes the general structure of Fig. 26 is all that matters.

The Auger neutralization process is represented in Fig. 26 as a vertical transition from the initial state curve 1 to some suitable final state curve. The vertical transition (constant s) expresses the fact that the Franck-Condon principle holds for these transitions. This principle also demands that $E_k(He^+)$ just before transition is equal to $E_k(He)$ just after. The result of these conditions is that the kinetic energy, $E_k(e^-)$, of the free electron e^- in the final state *outside* the solid is given by the vertical distance between curve 1 and a final state curve lying below it. The value of $E_k(e^-)$ indicated in Fig. 26 is for a transition from curve 1 to curve 4 occurring at the maximum $(s=s_m)$ of curve 6. Maximum $E_k(e^-)$ is obtained in transitions from curve 1 to curve 2.

Final states which lie below curve 1 at any s will give rise to electrons which can leave the solid. These are the transitions for which $\epsilon_k > \epsilon_0$ or $E_k > 0$ in Fig. 2. Final states lying between curves 1 and 5 correspond to allowed Auger transitions for which the excited electron cannot leave the solid $(\epsilon_c < \epsilon_k < \epsilon_0)$. Final states between curves 3 and 5 are forbidden because they re-

quire the excited electron to lie either in the forbidden gap or in the already filled valence band ($\epsilon_k < \epsilon_c$). These statements may be compared with the energy limits stated in Sec. III.

We may now obtain an expression for $E_i'(s)$ from the value of $[E_k(e^-)]_{\max}$, the vertical distance at any s between curves 1 and 2. This is equal to $E_i - 2(\epsilon_0 - \epsilon_v) + E(i,S) - E(n,S)$ from Fig. 26. But $[E_k(e^-)]_{\max}$ also equals $E'(s) - 2(\epsilon_0 - \epsilon_v)$ from Eq. (4). These facts lead to the following expression for the difference between the free space and effective ionization energies:

$$E_i - E_i'(s) = E(n,S) - E(i,S) = (\kappa-1)l^2/4(\kappa+1)s - B_i \exp(-b_i s) + B_n \exp(-b_n s). \quad (92)$$

In this expression evaluation of the ionic and atomic repulsive energy terms at the same value of s is justified by the Franck-Condon principle.

Equation (92) may be shown to lead to an expression for $E_i - E_i'$ in terms of ion energy like the empirical formula (27) found to fit the experimental data. If we assume that the Auger process occurs at $s = s_m$ given by Eq. (44) and that $b_n = b_i = b$, and use $\kappa = 16$ for germanium, we obtain

$$E_i - E_i'(s_m) = 3.2/s_m + B \exp(-b s_m) = 3.2a/\ln(A/av_0) + B(av_0/A)^{b/a}, \quad (93)$$

in which $B = B_n - B_i$ in ev, s_m and b^{-1} are in angstrom units. The first term in (93) is the image force interaction and varies slowly with s_m or v_0. We shall write it as a constant, $K_1 = 3.2/\bar{s}_m$, where $\bar{s}_m$ is a mean value for s_m over the v_0 range in question. v_0 will then be proportional to $(E_k + K_1)^{\frac{1}{2}}$ where E_k is the incident kinetic energy. If it is further true that $b \simeq a$, Eq. (93) may finally be written as

$$E_i - E_i' = K_1 + K_2(E_k + K_1)^{\frac{1}{2}}, \quad (94)$$

which becomes the empirical formula (27) if $K_1 = 2$ and $K_2 = 0.06$.

The above discussion indicates how the second conclusion listed in Sec. X could result from more basic considerations. The third conclusion in Sec. X concerns energy broadening and indicates that the over-all broadening parameter σ varies linearly with v_0 or $(E_k + K_1)^{\frac{1}{2}}$. We have seen that σ comprises two components σ_1 and σ_2, given for exponential rate function by Eqs. (85) and (88) and compounded according to Eq. (81). If Heisenberg broadening (σ_2) predominates Eq. (88) justifies the empirical result [Eq. (28)] directly. If σ_1 contributes we must determine its dependence on v_0 through $[dE_i'/ds]_{s=s_m}$.

Differentiating Eq. (92) yields

$$dE_i'/ds = (\kappa-1)e^2/4(\kappa+1)s^2 - b_i B_i \exp(-b_i s) + b_n B_n \exp(-b_n s). \quad (95)$$

Evaluating this expression at $s = s_m$, with $\kappa = 16$, $b_i = b_n = b$, and $B = B_n - B_i$ as before, we obtain

$$[dE_i'/ds]_{s=s_m} = 3.2/s_m^2 + bB \exp(-b s_m) = 3.2a^2/[\ln(A/av_0)]^2 + bB(av_0/A)^{b/a}. \quad (96)$$

σ_1 [Eq. (85)] will thus be linear in v_0 if $b \simeq a$ and if the second term in (96) predominates. Comparison with Eqs. (93), (94), and (27) taking $b \simeq 5$ A^{-1} indicates that the two terms in (96) are about equal for 10-ev ions and that the second term increases to about 10 times the first at 1000 ev. Thus σ_1, and hence σ, will be approximately linear in v_0 at the higher ion energies where broadening is important and the empirical result of Eq. (28) also appears justified in terms of the more basic elements of the problem.

It was pointed out in the work on metals[5] that for most any interatomic repulsive interaction, whether between free atoms or between atoms or ions in a crystal lattice, the coefficient of distance in the exponent is of the order of 5 A^{-1}. It was also shown that an estimate of a in the exponential rate function based on the overlap of exponential wave functions gives a value of about the same magnitude. This is not unreasonable since both the repulsive interaction and the Auger matrix element depend on overlap of the same wave functions.

There remains to discuss the magnitude of σ at 10 ev. Equations (93), (94), and (96) may be used with (85) to obtain

$$\sigma_1 = (0.53/a)[(K_1^2/3.2) + b(E_i - E_i' - K_1)]. \quad (97)$$

If we make the reasonable assumption that $b = a = 5$ A^{-1}, use $K_1 = 2$ and $E_i - E_i'$ from Table V we obtain $\sigma_1 \simeq 0.2$ ev. σ_2 is also about 0.2 ev from Eq. (88) which makes $\sigma \sim 0.3$ ev using Eq. (81), in agreement with what was found from the fit to the experimental $N_0(E_k)$ distribution.

The above discussion and the potential energy diagram on which it is based illuminate the possibilities with respect to distance from the surface at which the ion undergoes Auger neutralization. Comparison of Eqs. (94) and (27) indicates that at 10 ev, $E_i - E_i'$ is accounted for predominantly by the image force term with repulsive interaction contributing little. This indicates that at 10 ev the ion is neutralized at such distance from the surface where the repulsive interaction is just beginning to be felt. This is shown in Fig. 26 in the placement of curve 6 relative to curve 2. This must mean that s_m for 10-ev ions is about 2 A or about half the sum of the nearest neighbor distance in the semiconductor (2.2 A) and the viscosity diameter of the He atom (also 2.2 A). This result justifies the view that the Auger process occurs close to the solid at position B in Fig. 23. As ion energy increases Eqs. (94) and (27) indicate that to account for the further change in $E_i - E_i'$ one must include the repulsive interaction as neutralization occurs closer to the surface.

We may also conclude from the width and position

of the P_t function that all ions are neutralized before striking the lattice (Fig. 26). By Eq. (46) the width of the P_t function is $2.48/a=0.5$ A for $a=5$ A^{-1}. Thus we expect all 10-ev He^+ ions to be neutralized within ± 0.5 A of the mean position of ~ 2 A.

It is observed that the parameters A (or s_m), a, B_n, b_n, B_i, and b_i could be derived from Eqs. (44), (81), (85), (88), (92), and (95) using values of $E_i'(s_m)$ and σ determined by fitting experimental $N_0(E_k)$ distributions at a series of ion energies. The parameters used in drawing Fig. 26, which do not differ greatly from those used in the above discussion, were obtained in this way. The results must be considered preliminary because they were based on Gaussian broadening which we have seen can be improved upon for the higher ion energies.

XV. PROBABILITY OF ESCAPE

Equations (39) and (40) indicate, in agreement with Eq. (25), that the external distribution in electron energy, $N_0(\epsilon_k)$ is obtained from the internal distribution, $N_i(\epsilon_k)$, by multiplying by the probability of electron escape, $P_e(\epsilon_k)$. Using Eq. (82) for $N_i(\epsilon_k)$, we may write

$$N_0(\epsilon_k)=P_e(\epsilon_k)G'N_c(\epsilon_k)T_b[\tfrac{1}{2}(\epsilon_k+\epsilon_0-E_i'(s_m))]. \quad (98)$$

Here G' is the normalization factor in (82) given by:

$$1/G'=\int_{\epsilon_c}^{\infty} N_c(\epsilon_k)T_b[\tfrac{1}{2}(\epsilon_k+\epsilon_0-E_i'(s_m))]d\epsilon_k. \quad (99)$$

G' differs from G of Eq. (21) only by virtue of the inclusion of the final-state density function, $N_c(\epsilon_k)$.

In Eq. (98) we call attention to four gentle variations with energy ϵ_k which result if minor changes are made in (1) the specific form of the $P_e(\epsilon_k)$ function as distinguished from its general level and form, (2) the specific form of the $N_c(\epsilon_k)$ function, again as distinguished from its general level which is taken care of by the normalization factor G', (3) the specific form chosen for the $N_v(\epsilon)$ functions of Eqs. (6)–(10), and/or (4) the specific form chosen for the $q(\epsilon)$ function of Eqs. (14) and (15). The functions $q(\epsilon)$ and $N_v(\epsilon)$ are involved in T_b of Eq. (98) as indicated in Eqs. (13), (16), and (80). What is of interest here is that $q(\epsilon)$ may not be strictly linear as assumed nor $N_v(\epsilon)$ built up of exact parabolas. Minor changes in the forms of $P_e(\epsilon_k)$, $N_c(\epsilon_k)$, $q(\epsilon)$, and $N_v(\epsilon)$ all amount to gentle variations with energy ϵ_k in Eq. (98) which cannot be separated. For this reason we carry $N_c(\epsilon_k)$ no further in the calculation and revert to the definition of $N_0(\epsilon_k)$ given in Eqs. (25), (19), and (21). The probability of escape is still to be defined by Eq. (40) with the understanding that it may contain gentle variations with energy introduced by the specific choices of $q(\epsilon)$ and $N_v(\epsilon)$, and the assumption that $N_c(\epsilon_k)$ is constant. This is the only way in which the uniqueness of the theoretical fit is compromised. It can be said categorically that this can have only a minor effect on the basic conclusions concerning the parameters of the problem.

By Eq. (40), $P_e(\epsilon_k)$ is seen to depend both upon the angular variation of the matrix element specified by P_Ω in Eq. (66) and the critical angle for escape over the surface barrier, $\theta_c(\epsilon_k)$. If the matrix element, and hence the $N_i(\epsilon_k)$ distribution, is isotropic, then

$$P_\Omega(\theta,\epsilon_k,s_m)=1/4\pi. \quad (100)$$

It is then true for any barrier having cylindrical symmetry about the $\theta=0$ normal through the atom that

$$P_e(\epsilon_k)=\tfrac{1}{2}[1-\cos\theta_c(\epsilon_k)]. \quad (101)$$

If the barrier is plane and P_Ω isotropic, θ_c is given by

$$\theta_c(\epsilon_k)=\cos^{-1}(\epsilon_0/\epsilon_k)^{\frac{1}{2}}, \quad (102)$$

which from (101) results in the $P_e(\epsilon_k)$ function given in Eq. (22). We have concluded from the theoretical fit (item 4 in Sec. X) that this probability of escape is too small by a factor of several times unity. It is our purpose here to see what the general theory we have been developing has to say on this point. Clearly, one can depart from Eq. (22) either if P_Ω is anisotropic or if θ_c is greater than that characteristic of plane barrier [Eq. (102)]. Both effects are most likely operative.

We discuss first the anisotropy of $P_\Omega(\theta,\epsilon_k,s_m)$. We have seen in connection with Eq. (63) that the matrix element is the Coulomb interaction between a charge cloud $eF(1)=eu_g^*(1)u_v'(1)$ and another cloud $eG(2)=eu_e^*(2)u_v''(2)$. $F(1)$ is limited to the vicinity of the atom by $u_g^*(1)$. $G(2)$ may take on two different forms, one involving the u_e function of Fig. 23 for electrons which pass over the surface barrier and the other involving u_e' for electrons which are internally reflected. Over the volume of integration about the atom dictated by the $1/r_{12}$ interaction, the matrix element involving u_e will be greater than that involving u_e'. This will be true even though u_e oscillates through as many as several cycles in the volume of integration. Such oscillation is expected since the wavelength of a 6 ev electron is 1.6 A. Its effect is to reduce the transition probability over that which would be obtained for longer wavelength. However, we do not expect this effect to be as large as replacing an oscillatory u_e with an exponentially decaying u_e'. Thus the matrix element for $\theta<\theta_c$ is expected to be greater than that for $\theta>\theta_c$. If we take its value to be constant in these ranges, i.e., to have the value H_1 for $\theta<\theta_c$ and H_2 for $\theta>\theta_c$, then P_Ω will have the form shown in Fig. 27. We may take H_1 and H_2 to be the suitable average values of the matrix elements in the two angle ranges. Putting

$$H_1=fH_2, \quad f>1, \quad (103)$$

it follows that

$$P_{\Omega 1}=f^2P_{\Omega 2}, \quad (104)$$

with

$$\begin{aligned} P_{\Omega 1}&=(1/4\pi)[1-\alpha\cos\theta_c]^{-1}, \quad \theta<\theta_c,\\ P_{\Omega 2}&=(1-\alpha)P_{\Omega 1}, \quad \theta>\theta_c, \end{aligned} \quad (105)$$

in which

$$\alpha=1-1/f^2. \tag{106}$$

The resulting escape probability is

$$P_e(\epsilon_k)=\tfrac{1}{2}(1-\cos\theta_c)/(1-\alpha\cos\theta_c), \tag{107}$$

for any cylindrically symmetrical barrier. Equation (107) for a plane barrier [Eq. (102)] reduces to Eq. (23). P_Ω in the form of (105) could depend on s_m through f if f varied with distance. This variation must be small because use of the same $P_e(\epsilon_k)$ function for the $N_0(E_k)$ distributions plotted in Fig. 10 for five different incident energies, and hence s_m values, showed no significant departure from the experimental measurements in the variation of total yield with ion energy (Fig. 9). If the large escape probability were attributed entirely to anisotropy of P_Ω, then α in Eq. (23) must have a value of 0.956 (curve 2 of Fig. 15) for He^+ on Ge(111). By Eq. (106) this requires a ratio of matrix elements f in Eq. (103) of 4.8.

The second factor which can contribute to an escape probability larger than that of Eq. (22) arises from the bulge in the surface barrier caused by the potential well of the neutralized ion outside the surface. This bulge in the equi-energy surfaces outside the solid is cylindrically symmetrical about the surface normal through the atom. This leads to a greater critical angle $\theta_c(\epsilon_k)$ than that of Eq. (102) for the plane barrier. Either Eq. (101) for isotropic P_Ω or (107) for anisotropic P_Ω will give higher $P_e(\epsilon_k)$ for larger θ_c. Classical orbit calculations have been made for electrons starting along radii through the atom and moving in the image field of reasonable approximations to the solid surface and surface bulge. These result in appreciable increases in $\theta_c(\epsilon_k)$. In the actual case the electron orbits certainly do not all pass through the center of the atom. Electrons may be thought to originate throughout a volume about the atom in which the Coulomb interaction of the matrix element has value. The larger this volume, the less will be the effect produced by the bulge in the equi-energy surfaces about the atom. It is not possible without detailed calculations to determine the relative magnitude of the effects of P_Ω anisotropy and of the bulge in the surface barrier. But these are the possible reasons why $P_e(\epsilon_k)$ is several times larger than what Eq. (22) specifies. Total electron yield is thus not determined, as assumed by Shekhter,[3] by integrated transition probability over all distances, which is unity as we have seen. γ_i is determined by the escape probability and the fraction of the $N_i(\epsilon_k)$ distribution which lies above the vacuum level.

TABLE VI. Parameters concerning the state density functions in the valence bands of Si and Ge.

	ϵ_v[a]	p	$(1-p)\epsilon_v$[b]
Si	14–16	0.68	5.1
Ge	14–16	0.73	4.3

[a] Over-all width of the valence band in ev.
[b] Width of the degenerate p band in ev.

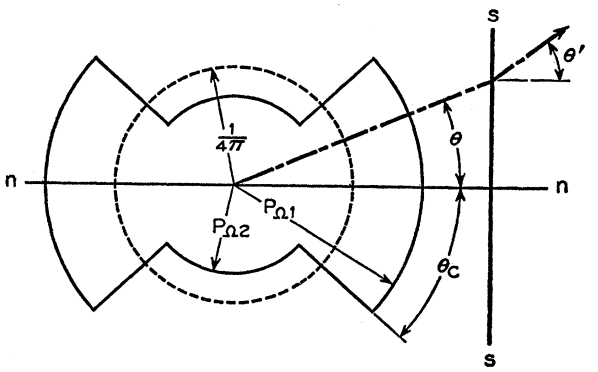

FIG. 27. Polar plot of the probability distribution $P_\Omega(\theta,\epsilon_k,s_m)$. The P_Ω surface is a figure of revolution about the surface normal $n-n$. $P_\Omega=1/4\pi$ is indicated by the dashed circle. The full contour indicates the distribution of Eq. (105). Refraction of the electron trajectory from θ to θ' at the surface is shown. θ_c is the critical angle for which $\theta'=\pi/2$.

Other one-parameter $P_e(\epsilon_k)$ functions like Eq. (23) were derived in the work on metals.[5] The two-parameter function [Eq. (24)], used extensively in this work, permits some freedom of choice of curvature of $P_e(\epsilon_k)$ thus making it possible to take account of the gentle variations with energy of $N_v(\epsilon)$, $q(\epsilon)$, and $N_c(\epsilon_k)$ which $P_e(\epsilon_k)$ comprises. We have thus completed our discussion of the four conclusions listed in Sec. X which the fit of theory to experiment has forced upon us.

XVI. LEVEL DENSITIES IN THE GERMANIUM AND SILICON VALENCE BANDS

The fit of the present theory to experiment provides a level density function, $N_v(\epsilon)$, in the valence bands of germanium given by curve 1 in Fig. 4. It is determined by the two parameters ϵ_v and p. ϵ_v is the total width and $(1-p)\epsilon_v$ is the width of the degenerate p bands. The accuracy with which we can determine the width of the p bands, even though this width is expressed as $(1-p)\epsilon_v$, does not depend upon the accuracy with which we know ϵ_v. Having picked a value for ϵ_v, $(1-p)\epsilon_v$ is adjusted until the higher energy peak of the experimental $N_0(E_k)$ is matched. Figure 12 shows that a change of ±0.015 in p is certainly discernible. This corresponds to an uncertainty in the p band width of ±0.3 ev. However, ϵ_v must be in a range in which a good fit to the experimental data is possible before $(1-p)\epsilon_v$ can be trusted as good value of the width of the degenerate p bands. This width is 4.3 ev for Ge, 5.1 ev for Si (Table VI).

The over-all width of the valence band is determined with less accuracy than the width of the p bands. The reason for this is that ϵ_v is so large relative to $E_i'(He^+)$ that valence electrons near $\epsilon=0$ cannot be raised above the vacuum level. The value of ϵ_v does affect the ability to fit the $N_0(E_k)$ distribution of electrons which do escape, however, and it is from this fact that a value

for ϵ_v is obtained. In a sense, this amounts to an extrapolation of $N_v(\epsilon)$ to the bottom of the band. The value of ϵ_v obtained should thus be more sensitive to the specific functions used for $N_v(\epsilon)$ than is $(1-p)\epsilon_v$.

We have seen in connection with Figs. 17 and 18 that one cannot fit the data well for ϵ_v much below 14 ev for germanium. Similar results, although somewhat less critical, are obtained for silicon. No systematic attempt to fit the data for $\epsilon_v > 16$ ev has been made, although it was shown that a reasonable fit for $\epsilon_v = 18$ ev could be obtained for Si. It was indicated in Sec. IX that a lower bound of 15 ev for ϵ_v for both Si and Ge exists if the disparity in theoretical and experimental γ_i for Ne^+ can be attributed to resonance tunneling from the valence band into the ground state of the atom. Consideration of all these facts leads to the conclusion that ϵ_v most likely lies in the range 14–16 ev for both Si and Ge (Table VI).

Soft x-ray results for Si have been extended recently by Kern[23] who has also re-evaluated earlier work. His Table II shows that ϵ_v from soft x rays lies in the range 13 to 16 ev in good agreement with the present results. Since the L emission indicates only the s electrons in $N_v(\epsilon)$ and the K emission only the p electrons, the sum of the L- and K-emission curves should give something like the $N_v(\epsilon)$ curve obtained in this work. Comparison of curve 1, Fig. 4 with the curves given in Kern's Fig. 5 show this, indeed, to be the case. The soft x-ray results for Ge[24] have been interpreted as giving ϵ_v near 7 ev and are thus in disagreement with the present work.

Several theoretical calculations of the band structure of silicon and germanium have been carried out.[10,25–27] Of these, the most recent and most accurate is that of Kleinman and Phillips.[27] Using a momentum-independent potential they find $\epsilon_v = 10.3$ ev. Their bands are close to those of a free-electron gas which, for the electron density of Si, has a Fermi energy of 11.5 ev. Kleinman and Phillips also quote a value of $\epsilon_v = 20.3$ ev obtained from a momentum-dependent exchange potential of a free-electron gas. Phillips[28] expects that screening effects of correlation will greatly reduce momentum-dependent effects leading to a total bandwidth which is larger than 10.3 ev by no more than 2 or 3 ev. Phillips[28] considers the difference between this theoretical ϵ_v of 12–13 ev and the 14–16 ev value reported here in Table VI to be significant. He would attribute the difference to the effect of the form of $N_v(\epsilon)$ used in the present work on the determination of the total bandwidth as discussed above. Because the electron densities in Si and Ge differ by less than 10%, ϵ_v is expected to be the same within about 10% for the two crystals. This is in accord with present work but not with the soft x-ray results.

A theoretical estimate of the width of the degenerate p bands requires that one know the position in the Brillouin zone of the point in this band which lies lowest in energy. Phillips[29] found the lowest lying point in Si to be $W_2^{(1)}$ and considers this to be close to the bottom of the degenerate p band because of the very close agreement between his results[10,29] and those of Kleinman and Phillips.[27] The theoretical p bandwidth is then 4 ev with an uncertainty of ± 1 ev.[27] Similar results are expected for Ge. The experimental values of 5.1 and 4.3 ev for Si and Ge, respectively, are thus in good agreement with the latest theoretical estimates. The Si result appears to agree with the evidence of the degenerate p bands in the K-emission results of Kern.[23]

The present work suggests more strongly than did that for metals that Auger electron ejection may be used to determine state densities in the filled bands of solids generally. Experimentally, the chief problem is the production of atomically clean surfaces. In extracting the state density function from the experimental kinetic energy distribution one must work through an integral transform. In the present work one chooses $N_v(\epsilon)$ and works through the integral transform in the "forward" direction to fit $N_0(E_k)$. This requires that something be known *a priori* about the form of $N_v(\epsilon)$ as is the case for the diamond-type semiconductors. A more general application of Auger ejection to the determination of state density functions will require a method of deriving $N_v(\epsilon)$ from $N_0(E_k)$ directly without any assumptions as to its form.

XVII. SURFACE EFFECTS

The experimental results and theory of Auger neutralization at a semiconductor provide several interesting implications or conclusions about the surfaces of these solids. Since the ion is neutralized outside the solid, the electrons involved are surface electrons and the conditions under which the Auger process proceeds are surface conditions. Thus one must take into account (1) the existence of surface states in the energy gap, (2) the fact that the level density distribution and hybridization of the valence band involved in the Auger process are those prevailing at the surface, and (3) the difference between electrostatic potential at the surface and in the bulk caused by occupancy of the surface states and the possible existence of a chemical doping layer in the surface layers of the crystal.

Electrons residing in surface states in the energy gap should partipate in the Auger neutralization process and produce a tail on the high-energy end of the $N_0(E_k)$ distribution above the energy limit calculated by Eq. (4). The experimental $N_0(E_k)$ distribution when compared with the broadened theoretical curve in Fig. 8

[23] B. Kern, Z. Physik **159**, 178 (1960).
[24] D. H. Tomboulian and D. E. Bedo, Phys. Rev. **104**, 590 (1956).
[25] F. Herman, Physica **20**, 801 (1954).
[26] T. O. Woodruff, Phys. Rev. **103**, 1159 (1956); in *Solid State Physics*, edited by F. Seitz and D. Turnbull (Academic Press, Inc., New York, 1957), Vol. IV, p. 367.
[27] L. Kleinman and J. C. Phillips, Phys. Rev. **118**, 1153 (1960).
[28] J. C. Phillips (private communication).
[29] J. C. Phillips, J. Phys. Chem. Solids 8, 369 (1959).

shows very little evidence of such a tail. This may result if the surface density of electrons in such states is small compared to the surface density of $\sim 4\times 10^{15}$ valence electrons per cm. It could also result if the wave function of the surface state does not extend as far from the solid as do the p functions which characterize the top of the valence band. Recent estimates[30–32] indicate that the surface density of electrons in surface states necessary to account for the observed bending of bands at the atomically clean surface lie in the range 10^{12}–10^{13} per cm^2 or more. This may, in fact, be above the limit of what should be observable if the wave functions of the surface states extend from the surface in a manner comparable to the p electrons at the top of the valence band. If the results of Koutecký and Tomášek[33,34] concerning rehybridization of surface orbitals are valid, one expects an enhanced probability of Auger neutralization involving electrons in surface states in possible disagreement with the present work. A definitive statement concerning the role of filled surface states cannot be made until their density has been fixed with greater precision.

All of the results of the present work indicate that the surface level density distribution and the surface hybridization of the valence band are close to those expected for the bulk. One cannot accommodate any serious distortion at the surface. It should be pointed out, however, that this statement need not preclude some surface rehybridization if it involves admixture of orbitals of higher angular momentum than s and p leaving the ratio of s to p and its variation through the band close to that in the bulk. The magnitude of orbitals of higher angular momentum will be quite small near the atom outside the surface as the functions of Fig. 24 indicate. The conclusions reached here concerning the relation of the surface level density distribution to that in the bulk do not agree with the suggestions of Handler.[31,32]

We expect a difference in electrostatic potential between surface and bulk to have essentially no effect on the Auger neutralization process. Electrons involved in the Auger process come from the outermost surface layer only and no averaging over the space charge layer occurs. Values of surface energies such as $\epsilon_0-\epsilon_v$ used in this work were determined for the surface and thus introduce no error (Table II). States within a few tenths of an electron volt of the top of the valence band will no longer communicate with the bulk of the solid if the energy bands bend up at the surface by this amount. This apparently produces such a small change in wave function over such a narrow energy range as to be unobservable in this work.

[30] A. B. Fowler, J. Appl. Phys. **30**, 556 (1959).
[31] P. Handler and W. M. Portnoy, Phys. Rev. **116**, 516 (1959).
[32] P. Handler, J. Phys. Chem. Solids **14**, 1 (1960).
[33] J. Koutecký, J. Phys. Chem. Solids **14**, 233 (1960).
[34] J. Koutecký and M. Tomášek, J. Phys. Chem. Solids **14**, 241 (1960).

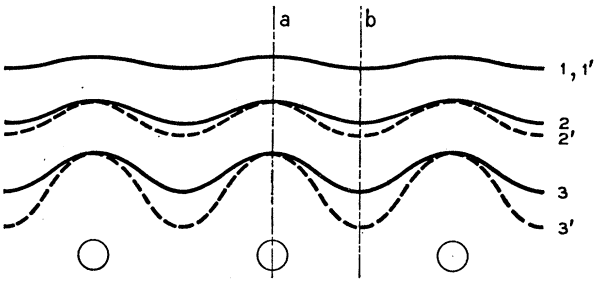

FIG. 28. Plot showing intersections which surfaces of constant transition rate and constant effective ionization energy might make with a plane perpendicular to the solid surface passed through a row of surface atoms (open circles).

Some comment should also be made concerning possible effects of surface atomicity. A possible dependence on azimuthal angle was pointed out in Sec. XII which was assumed to average out to independence of φ on integration over the surface. Also the sp^3 hybridization at the surface need only be an average permitting variation in either direction near individual atoms or between atoms of the surface. Surface atomicity could also have an effect on energy broadening which is now discussed.

We consider the differences to be expected as we vary the impact parameter relative to a surface normal projecting, say, from a given surface atom. The important consideration here is the way in which contours of constant transition rate, $R_t(s)$, vary with respect to those of constant effective ionization energy, $E_i'(s)$, over the solid surface as s decreases. If the solid surface were an ideal structureless plane, the contours of constant R_t and E_i' would be planes and R_t and E_i' would bear the same relation to each other at all points on the surface. If the surface is made up of atoms, the surfaces of constant R_t and E_i' undulate with the surface periodicity of atoms and may not have the same form for all distances s as is indicated in Fig. 28. Here are shown the intersections of possible contours of constant R_t and E_i' with a plane perpendicular to the surface which passes through a row of surface atoms. The surface atoms are indicated by the open circles. Let us suppose that 1, 2, 3 are contours of constant E_i' and 1′, 2′, 3′ contours of constant R_t. Under the circumstances depicted in Fig. 28 an ion coming in along the surface normal a will undergo transition at a point at which the effective ionization energy E_i' differs less from the free-space value E_i than for an ion approaching along the surface normal b. On a potential energy diagram like that of Fig. 26 drawn for the normal a, the P_t functions would lie farther from the surface relative to the potential curves than on a diagram drawn for the normal b. This might result in further energy broadening over what is expected when the possible deviation of energy and rate contours over the surface is neglected. For 10-ev ions an estimate of σ based on calculations of σ_1 and σ_2 accounts for the observed

magnitude of σ (Sec. XIV). We conclude that for 10-ev ions at least "surface broadening" of the type discussed here is small. Surface broadening could become important for faster ions if one were to attempt to evaluate the component contributions to the over-all broadening parameter σ.

XVIII. ACKNOWLEDGMENTS

The author is grateful for many stimulating discussions with a number of his colleagues. In particular, he would like to acknowledge the help of P. A. Wolff, C. Herring, G. H. Wannier, and J. C. Phillips. This work would, of course, have been impossible without the programming efforts of Mrs. Wanda Mammel, to whom the author expresses his sincere gratitude. Mrs. Mammel also performed the integration involved in the representations of the Auger transform of Tables VII, VIII, and IX. Thanks are also due Miss M. C. Gray for consultation on mathematical questions and to A. R. Hutson, P. Kisliuk, G. E. Moore, J. C. Phillips, and P. A. Wolff for critical reading of the manuscript.

XIX. APPENDIX

The details of the calculation of the Auger transform $T(\epsilon)$ of Eq. (16) are given here. The $N_v(\epsilon)$ and $q(\epsilon)$ functions used in the definition of $N_v'(\epsilon)$ in Eq. (13) are made up of the component functions $N_n(\epsilon)$ defined in Eqs. (6)–(10) and $q_n(\epsilon)$ defined in Eqs. (14) and (15), respectively. If we now let

$$M_n = q_n N_n / C_1, \tag{108}$$

$$\lambda = (1-r)/\epsilon_v, \tag{109}$$

and

$$\mu = r(1-p)^{-\frac{3}{2}}, \tag{110}$$

we obtain

$$M_1(\epsilon) = (1-\lambda\epsilon)\epsilon^{\frac{1}{2}}, \quad 0 \leq \epsilon \leq \epsilon_v/2, \tag{111}$$

$$M_2(\epsilon) = (1-\lambda\epsilon)(\epsilon_v-\epsilon)^{\frac{1}{2}}, \quad \epsilon_v/2 \leq \epsilon \leq p\epsilon_v, \tag{112}$$

$$M_3(\epsilon) = (1-\lambda\epsilon)(\epsilon_v-\epsilon)^{\frac{1}{2}} + \mu(\epsilon - p\epsilon_v)^{\frac{1}{2}}, \quad p\epsilon_v \leq \epsilon \leq (1+p)\epsilon_v/2, \tag{113}$$

and

$$M_4(\epsilon) = (1-\lambda\epsilon+\mu)(\epsilon_v-\epsilon)^{\frac{1}{2}}, \quad (1+p)\epsilon_v/2 \leq \epsilon \leq \epsilon_v. \tag{114}$$

A convenient function related to the Auger transform $T(\epsilon)$ of Eq. (16) is

$$S(\epsilon) = T(\epsilon)/C_1^2, \tag{115}$$

in which C_1 is the constant defined in Eq. (11). Then

$$S(\epsilon) = \int M(\epsilon-\Delta)M(\epsilon+\Delta)d\Delta. \tag{116}$$

$S(\epsilon)$ has been expressed analytically in terms of the $M_n(\epsilon)$ over the range of p values, $\frac{1}{2} \leq p \leq 1$. Three expressions are necessary, one for $\frac{1}{2} \leq p \leq \frac{2}{3}$, another for $\frac{2}{3} \leq p \leq \frac{3}{4}$, and a third for $\frac{3}{4} \leq p \leq 1$. Expressions for $S(\epsilon)$

TABLE VII. Expressions for $S(\epsilon) = T(\epsilon)/C_1^2$ in terms of sums of terms $S_{nm}(L_2,L_1)$.

	$S(\epsilon) = \sum S_{nm}(L_2,L_1)$	$\frac{1}{2} \leq p \leq \frac{2}{3}$	$\frac{2}{3} \leq p \leq \frac{3}{4}$	$\frac{3}{4} \leq p \leq 1$
1	$S_{11}[\epsilon,0]$	$0 \leq \epsilon \leq \frac{1}{4}\epsilon_v$	$0 \leq \epsilon \leq \frac{1}{4}\epsilon_v$	$0 \leq \epsilon \leq \frac{1}{4}\epsilon_v$
2	$S_{11}[\frac{1}{2}\epsilon_v-\epsilon,0]$	$\frac{1}{4}\epsilon_v \leq \epsilon \leq \frac{1}{2}p\epsilon_v$	$\frac{1}{4}\epsilon_v \leq \epsilon \leq \frac{1}{2}p\epsilon_v$	$\frac{1}{4}\epsilon_v \leq \epsilon \leq \frac{1}{2}p\epsilon_v$
3	$S_{11}[\frac{1}{2}\epsilon_v-\epsilon,0] + S_{12}[\epsilon,p\epsilon_v-\epsilon]$	$\frac{1}{2}p\epsilon_v \leq \epsilon \leq \frac{1}{4}(1+p)\epsilon_v$	$\frac{1}{2}p\epsilon_v \leq \epsilon \leq \frac{1}{4}(1+p)\epsilon_v$	$\frac{1}{2}p\epsilon_v \leq \epsilon \leq \frac{1}{4}(1+p)\epsilon_v$
4	$S_{11}[\frac{1}{2}\epsilon_v-\epsilon,0] + S_{12}[p\epsilon_v-\epsilon,\frac{1}{2}\epsilon_v-\epsilon] + S_{13}[\frac{1}{2}(1+p)\epsilon_v-\epsilon,p\epsilon_v-\epsilon] + S_{14}[\epsilon,\frac{1}{2}(1+p)\epsilon_v-\epsilon]$	$\frac{1}{4}(1+p)\epsilon_v \leq \epsilon \leq \frac{1}{2}\epsilon_v$	$\frac{1}{4}(1+p)\epsilon_v \leq \epsilon \leq \frac{1}{2}\epsilon_v$	$\frac{1}{4}(1+p)\epsilon_v \leq \epsilon \leq \frac{3}{8}\epsilon_v$
5	$S_{22}[\epsilon-\frac{1}{2}\epsilon_v,0] + S_{12}[p\epsilon_v-\epsilon,\epsilon-\frac{1}{2}\epsilon_v] + S_{18}[\frac{1}{2}(1+p)\epsilon_v-\epsilon,p\epsilon_v-\epsilon] + S_{14}[\epsilon_v-\epsilon,\frac{1}{2}(1+p)\epsilon_v-\epsilon]$	$\frac{1}{2}\epsilon_v \leq \epsilon \leq \frac{1}{4}(1+2p)\epsilon_v$	$\frac{1}{2}\epsilon_v \leq \epsilon \leq \frac{1}{4}(1+2p)\epsilon_v$	$\frac{1}{2}\epsilon_v \leq \epsilon \leq \frac{1}{4}(1+2p)\epsilon_v$
6	$S_{22}[p\epsilon_v-\epsilon,0] + S_{23}[\epsilon-\frac{1}{2}\epsilon_v,p\epsilon_v-\epsilon] + S_{18}[\frac{1}{2}(1+p)\epsilon_v-\epsilon,\epsilon-\frac{1}{2}\epsilon_v] + S_{14}[\epsilon_v-\epsilon,\frac{1}{2}(1+p)\epsilon_v-\epsilon]$	$\frac{1}{4}(1+2p)\epsilon_v \leq \epsilon \leq p\epsilon_v$	$\frac{1}{4}(1+2p)\epsilon_v \leq \epsilon \leq \frac{1}{4}(2+p)\epsilon_v$	$\frac{1}{4}(1+2p)\epsilon_v \leq \epsilon \leq \frac{1}{4}(2+p)\epsilon_v$
7	$S_{23}[\epsilon-p\epsilon_v,0] + S_{23}[\epsilon-p\epsilon_v,\epsilon-\frac{1}{2}\epsilon_v] + S_{18}[\frac{1}{2}(1+p)\epsilon_v-\epsilon,\epsilon-\frac{1}{2}\epsilon_v] + S_{14}[\epsilon_v-\epsilon,\frac{1}{2}(1+p)\epsilon_v-\epsilon]$	$p\epsilon_v \leq \epsilon \leq \frac{1}{4}(2+p)\epsilon_v$	...	...
7′	$S_{22}[p\epsilon_v-\epsilon,0] + S_{23}[\epsilon-\frac{1}{2}\epsilon_v,\frac{1}{2}(1+p)\epsilon_v-\epsilon] + S_{24}[\epsilon-\frac{1}{2}\epsilon_v,p\epsilon_v-\epsilon] + S_{14}[\epsilon_v-\epsilon,\epsilon-\frac{1}{2}\epsilon_v]$	...	$\frac{1}{4}(2+p)\epsilon_v \leq \epsilon \leq p\epsilon_v$	$\frac{1}{4}(2+p)\epsilon_v \leq \epsilon \leq \frac{3}{8}\epsilon_v$
8	$S_{23}[\epsilon-p\epsilon_v,0] + S_{23}[\frac{1}{2}(1+p)\epsilon_v-\epsilon,\epsilon-p\epsilon_v] + S_{24}[\epsilon-\frac{1}{2}\epsilon_v,\frac{1}{2}(1+p)\epsilon_v-\epsilon] + S_{14}[\epsilon_v-\epsilon,\epsilon-\frac{1}{2}\epsilon_v]$	$\frac{1}{4}(2+p)\epsilon_v \leq \epsilon \leq \frac{1}{2}(1+3p)\epsilon_v$	$p\epsilon_v \leq \epsilon \leq \frac{3}{4}\epsilon_v$	...
8′	$S_{22}[p\epsilon_v-\epsilon,0] + S_{23}[\frac{1}{2}(1+p)\epsilon_v-\epsilon,\frac{1}{2}(1+p)\epsilon_v-\epsilon] + S_{24}[\epsilon_p-\epsilon,\frac{1}{2}(1+p)\epsilon_v-\epsilon]$	...	...	$\frac{3}{4}\epsilon_v \leq \epsilon \leq p\epsilon_v$
9	$S_{23}[\frac{1}{2}(1+p)\epsilon_v-\epsilon,0] + S_{34}[\epsilon-p\epsilon_v,\frac{1}{2}(1+p)\epsilon_v-\epsilon] + S_{24}[\epsilon-\frac{1}{2}\epsilon_v,\epsilon-p\epsilon_v] + S_{14}[\epsilon_v-\epsilon,\epsilon-\frac{1}{2}\epsilon_v]$	$\frac{1}{4}(1+3p)\epsilon_v \leq \epsilon \leq \frac{3}{4}\epsilon_v$	...	...
9′	$S_{23}[\epsilon-p\epsilon_v,0] + S_{23}[\frac{1}{2}(1+p)\epsilon_v-\epsilon,\epsilon-p\epsilon_v] + S_{24}[\epsilon_v-\epsilon,\frac{1}{2}(1+p)\epsilon_v-\epsilon]$	...	$\frac{3}{4}\epsilon_v \leq \epsilon \leq \frac{1}{4}(1+3p)\epsilon_v$	$p\epsilon_v \leq \epsilon \leq \frac{1}{4}(1+3p)\epsilon_v$
10	$S_{23}[\frac{1}{2}(1+p)\epsilon_v-\epsilon,0] + S_{34}[\epsilon-p\epsilon_v,\frac{1}{2}(1+p)\epsilon_v-\epsilon] + S_{24}[\epsilon_v-\epsilon,\frac{1}{2}(1+p)\epsilon_v-\epsilon]$	$\frac{3}{4}\epsilon_v \leq \epsilon \leq \frac{1}{2}(1+p)\epsilon_v$	...	...
10′	$S_{23}[\frac{1}{2}(1+p)\epsilon_v-\epsilon,0] + S_{34}[\epsilon-p\epsilon_v,\frac{1}{2}(1+p)\epsilon_v-\epsilon] + S_{24}[\epsilon_v-\epsilon,\epsilon-p\epsilon_v]$	...	$\frac{1}{4}(1+3p)\epsilon_v \leq \epsilon \leq \frac{1}{2}(1+p)\epsilon_v$	$\frac{1}{4}(1+3p)\epsilon_v \leq \epsilon \leq \frac{1}{2}(1+p)\epsilon_v$
11	$S_{44}[\epsilon-\frac{1}{2}(1+p)\epsilon_v,0] + S_{34}[\epsilon_v-\epsilon,\epsilon-\frac{1}{2}(1+p)\epsilon_v]$	$\frac{1}{2}(1+p)\epsilon_v \leq \epsilon \leq \frac{1}{4}(3+p)\epsilon_v$	$\frac{1}{4}(1+p)\epsilon_v \leq \epsilon \leq \frac{1}{4}(3+p)\epsilon_v$	$\frac{1}{2}(1+p)\epsilon_v \leq \epsilon \leq \frac{1}{4}(3+p)\epsilon_v$
12	$S_{44}[\epsilon_v-\epsilon,0]$	$\frac{1}{4}(3+p)\epsilon_v \leq \epsilon \leq \epsilon_v$	$\frac{1}{4}(3+p)\epsilon_v \leq \epsilon \leq \epsilon_v$	$\frac{1}{4}(3+p)\epsilon_v \leq \epsilon \leq \epsilon_v$

TABLE VIII. Expressions for $S_{nm}(L_2,L_1)$ in terms of λ, μ, and the integrals $I_n(L_2,L_1,\alpha)$.

$$S_{11}(L_2,L_1)=(1-\lambda\epsilon)^2 I_1(L_2,L_1,\epsilon)-\lambda^2 I_2(L_2,L_1,\epsilon)$$

$$S_{12}(L_2,L_1)=[(1-\lambda\epsilon)^2-\tfrac{1}{4}\lambda^2\epsilon_v^2]I_4(L_2-\tfrac{1}{2}\epsilon_v,\ L_1-\tfrac{1}{2}\epsilon_v,\ \epsilon-\tfrac{1}{2}\epsilon_v)-\lambda^2 I_5(L_2-\tfrac{1}{2}\epsilon_v,\ L_1-\tfrac{1}{2}\epsilon_v,\ \epsilon-\tfrac{1}{2}\epsilon_v)-\lambda^2\epsilon_v I_6(L_2-\tfrac{1}{2}\epsilon_v,\ L_1-\tfrac{1}{2}\epsilon_v,\ \epsilon-\tfrac{1}{2}\epsilon_v)$$

$$S_{13}(L_2,L_1)=S_{12}+\mu(1-\lambda\epsilon+\tfrac{1}{2}\lambda p\epsilon_v)I_1(L_2-\tfrac{1}{2}p\epsilon_v,\ L_1-\tfrac{1}{2}p\epsilon_v,\ \epsilon-\tfrac{1}{2}p\epsilon_v)+\lambda\mu I_3(L_2-\tfrac{1}{2}p\epsilon_v,\ L_1-\tfrac{1}{2}p\epsilon_v,\ \epsilon-\tfrac{1}{2}p\epsilon_v)$$

$$S_{14}(L_2,L_1)=[(1-\lambda\epsilon)^2+\mu(1-\lambda\epsilon)-\lambda^2(\tfrac{1}{2}\epsilon_v)^2+\tfrac{1}{2}\lambda\mu\epsilon_v]I_4(L_2-\tfrac{1}{2}\epsilon_v,\ L_1-\tfrac{1}{2}\epsilon_v,\ \epsilon-\tfrac{1}{2}\epsilon_v)-\lambda^2 I_5(L_2-\tfrac{1}{2}\epsilon_v,\ L_1-\tfrac{1}{2}\epsilon_v,\ \epsilon-\tfrac{1}{2}\epsilon_v)$$
$$+\lambda(\mu-\lambda\epsilon_v)I_6(L_2-\tfrac{1}{2}\epsilon_v,\ L_1-\tfrac{1}{2}\epsilon_v,\ \epsilon-\tfrac{1}{2}\epsilon_v)$$

$$S_{22}(L_2,L_1)=(1-\lambda\epsilon)^2 I_1(L_2,L_1,\ \epsilon_v-\epsilon)-\lambda^2 I_2(L_2,L_1,\ \epsilon_v-\epsilon)$$

$$S_{23}(L_2,L_1)=S_{22}+\mu[1-\lambda\epsilon-\tfrac{1}{2}\lambda(1-p)\epsilon_v]I_4(L_2+\tfrac{1}{2}(1-p)\epsilon_v,\ L_1+\tfrac{1}{2}(1-p)\epsilon_v,\ \epsilon-\tfrac{1}{2}(1+p)\epsilon_v)$$
$$+\lambda\mu I_6(L_2+\tfrac{1}{2}(1-p)\epsilon_v,\ L_1+\tfrac{1}{2}(1-p)\epsilon_v,\ \epsilon-\tfrac{1}{2}(1+p)\epsilon_v)$$

$$S_{24}(L_2,L_1)=[\mu(1-\lambda\epsilon)+(1-\lambda\epsilon)^2]I_1(L_2,L_1,\ \epsilon_v-\epsilon)-\lambda^2 I_2(L_2,L_1,\ \epsilon_v-\epsilon)+\lambda\mu I_3(L_2,L_1,\ \epsilon_v-\epsilon)$$

$$S_{33}(L_2,L_1)=S_{23}+\mu^2 I_1(L_2,L_1,\ \epsilon-p\epsilon_v)+\mu[1-\lambda\epsilon-\tfrac{1}{2}\lambda(1-p)\epsilon_v]I_4(L_2-\tfrac{1}{2}(1-p)\epsilon_v,\ L_1-\tfrac{1}{2}(1-p)\epsilon_v,\ \epsilon-\tfrac{1}{2}(1+p)\epsilon_v)$$
$$-\lambda\mu I_6(L_2-\tfrac{1}{2}(1-p)\epsilon_v,\ L_1-\tfrac{1}{2}(1-p)\epsilon_v,\ \epsilon-\tfrac{1}{2}(1+p)\epsilon_v)$$

$$S_{34}(L_2,L_1)=S_{24}+\mu[1-\lambda\epsilon-\tfrac{1}{2}\lambda(1-p)\epsilon_v+\mu]I_4(L_2-\tfrac{1}{2}(1-p)\epsilon_v,\ L_1-\tfrac{1}{2}(1-p)\epsilon_v,\ \epsilon-\tfrac{1}{2}(1+p)\epsilon_v)$$
$$-\lambda\mu I_6(L_2-\tfrac{1}{2}(1-p)\epsilon_v,\ L_1-\tfrac{1}{2}(1-p)\epsilon_v,\ \epsilon-\tfrac{1}{2}(1+p)\epsilon_v)$$

$$S_{44}(L_2,L_1)=(1-\lambda\epsilon+\mu)^2 I_1(L_2,L_1,\ \epsilon_v-\epsilon)-\mu^2 I_2(L_2,L_1,\ \epsilon_v-\epsilon)$$

are of the form,

$$S(\epsilon)=\sum S_{nm}(L_2,L_1), \tag{117}$$

and are listed in Table VII. For each of the three ranges of p given above the energy range $0\leq\epsilon\leq\epsilon_v$ breaks up into 12 regions in each of which a different sum such as (117) is valid. The quantities L_1 and L_2 are the functions of ϵ, p, and ϵ_v given in Table VII. The $S_{nm}(L_2,L_1)$ terms are polynomials in λ and μ of Eqs. (109) and (110) and the definite integrals $I_n(L_2,L_1,\alpha)$ (Table VIII). These definite integrals are listed in Table IX. Here the quantities L_1 and L_2 to be found in Table VII appear as the limits of the integrals. The computer program calculates $S(\epsilon)$ over the energy range $0\leq\epsilon\leq\epsilon_v$ at equally spaced points separated by an interval usually taken to be 0.25 ev.

TABLE IX. Expressions for the integrals $I_n(L_2,L_1,\alpha)$.

$$I_1(L_2,L_1,\alpha)=\int_{L_1}^{L_2}(\alpha^2-x^2)^{\frac{1}{2}}dx$$
$$=\tfrac{1}{2}[x(\alpha^2-x^2)^{\frac{1}{2}}-\alpha^2\arctan x(\alpha^2-x^2)^{-\frac{1}{2}}]_{L_1}^{L_2}$$

$$I_2(L_2,L_1,\alpha)=\int_{L_1}^{L_2}x^2(\alpha^2-x^2)^{\frac{1}{2}}dx=\tfrac{1}{4}[\alpha^2 I_1-x(\alpha^2-x^2)^{\frac{3}{2}}]_{L_1}^{L_2}$$

$$I_3(L_2,L_1,\alpha)=\int_{L_1}^{L_2}x(\alpha^2-x^2)^{\frac{1}{2}}dx=-\tfrac{1}{3}[(\alpha^2-x^2)^{\frac{3}{2}}]_{L_1}^{L_2}$$

$$I_4(L_2,L_1,\alpha)=\int_{L_1}^{L_2}(x^2-\alpha^2)^{\frac{1}{2}}dx=\tfrac{1}{2}[x(x^2-\alpha^2)^{\frac{1}{2}}-\alpha^2\ln(x+(x^2-\alpha^2)^{\frac{1}{2}})]_{L_1}^{L_2}$$

$$I_5(L_2,L_1,\alpha)=\int_{L_1}^{L_2}x^2(x^2-\alpha^2)^{\frac{1}{2}}dx=\tfrac{1}{4}[\alpha^2 I_4+x(x^2-\alpha^2)^{\frac{3}{2}}]_{L_1}^{L_2}$$

$$I_6(L_2,L_1,\alpha)=\int_{L_1}^{L_2}x(x^2-\alpha^2)^{\frac{1}{2}}dx=\tfrac{1}{3}[(x^2-\alpha^2)^{\frac{3}{2}}]_{L_1}^{L_2}$$

The broadened $S(\epsilon)$ function called $S_b(\epsilon)$ and the change of variable from ϵ to ϵ_k are carried out by a formula analogous to Eq. (17). $N_i(\epsilon_k)$ is then

$$N_i(\epsilon_k)=GS_b[\tfrac{1}{2}(\epsilon_k+\epsilon_0-E_i'(s_m))], \tag{118}$$

in which G is the normalizing factor given by

$$1/G=\int_{\epsilon_c}^{\infty}S_b[\tfrac{1}{2}(\epsilon_k+\epsilon_0-E_i'(s_m))]d\epsilon_k$$
$$=2\int_{\frac{1}{2}[\epsilon_c+\epsilon_0-E_i'(s_m)]}^{\epsilon_v}S_b(\epsilon)d\epsilon. \tag{119}$$

Equations (118) and (119) are the analogs of Eqs. (19) and (21), respectively.